EXPERIMENTAL AND THEORETICAL APPLICATION OF FAULT IDENTIFICATION MEASURES OF ACCURACY IN ROTATING MACHINE DIAGNOSTICS

ANDREA VANIA AND PAOLO PENNACCHI

Dipartimento Di Meccanica,
Politecnico di Milano,
Via La Masa 34, I-20158 Milano
andrea.vania@polimi.it, paolo.pennacchi@polimi.it

Running title: ACCURACY OF FAULT IDENTIFICATION

Please send proofs to
PROF. PAOLO PENNACCHI
Dipartimento Di Meccanica,
Politecnico di Milano,
Via La Masa 34, I-20158 Milano

ABSTRACT

Model based diagnostic techniques can be used successfully in the health analysis of rotormachinery. Unfortunately, a poor accuracy of the model of the fully assembled machine, as well as errors in the evaluation of the experimental vibrations caused only by the impending fault, can affect the accuracy of fault identifications. This can make difficult to identify the type of the actual fault as well as to evaluate its severity and its position. This paper shows some methods that have been developed to measure the accuracy of the results obtained with model based techniques aimed to identify faults in rotating machines. The testing of the capabilities of these methods is carried out using both machine response simulated with mathematical models and experimental data on a real machine.

1. INTRODUCTION

The early detection of faults and malfunctions in rotating machines can be provided by condition monitoring. This is very important to avoid the development of faults and then to avoid a more serious damage to occur. The opportunity to carry out a predictive maintenance allows repair costs to be reduced as the primary fault is detected during the first stage of its development and secondary induced faults are avoided. However, in order to obtain useful information to carry out suitable maintenance actions, a fault diagnosis is required. A first preliminary screening of the types of faults that can have generated an alarm can be obtained with a fault symptom analysis [1-2] and applications can be found also in rotordynamics field [3-5]. However, more significant information can be provided by model based diagnostic techniques [6-11]. These methods allow the fault to be localised and its severity to be evaluated. Usually, the model of the fully assembled machine allows the dynamic behaviour of the rotors, the bearings and the foundation to be simulated [12].

The identification of a fault can be obtained by evaluating the system of excitations that minimises the error, called *residual*, between the machine experimental response and the numerical response evaluated with the model. In order to allow the results of different analyses to be compared the residuals are normalised. Weighted least square methods can be used to identify the equivalent forces and moments that simulate the faults (see also [13]). Some methods are applied in the time domain [14-16], but most of the fault identification methods are developed in frequency domain, as done by the authors in many previous applications [7-8, 12, 17] and as considered in this paper.

As all the model based identification methods, also the least square identification method in frequency domain could be affected by errors and the results could not be accurate. Some causes of inaccuracy are listed in the following:

- Limited number of measurement points of vibrations: in real rotating machines, only shaft and support vibrations measured at the journal bearings are available; this reduces the number of information that can be used in the identification procedure.
- Lack of accuracy of the machine model (modelling errors): whilst the model of the rotor only is generally reliable, errors in the bearing coefficients or in the foundation parameters are not unusual. These could be due e.g. to different alignment conditions of the machine that determine an oil film thickness in the bearings different from that used for the calculation of stiffness and damping coefficients or to a different temperature of the oil temperature at the inlet. These effects cannot be easily modelled as they are generally unknown.
- Errors in the evaluation of the vibrations caused only by the fault that must be identified: machine vibrations are not null even in normal conditions, owing to the presence of a residual bow and unbalance. Then the occurrence of a fault causes *additional vibrations*. In order to identify the fault, it is important to analyse the additional vibrations only and not the raw data collected by the condition monitoring system. These additional vibrations, induced only by the fault that must be identified, can be evaluated by subtracting the transient vibration vectors (1x rev., 2x rev., …) measured after the fault occurrence from the respective vibration vectors previously measured, in normal condition. Obviously, this approach considers the system to be linear and time invariant. Errors in the evaluation of these additional vibrations cause lack of accuracy. For instance, the thermal conditions of the two transients used to evaluate the additional vibrations could not be the same. Anyhow, a careful choice of the transient vibrations can reduce these errors significantly.
- Random / bias errors in the vibration data: another cause of error can be the presence of noise in the vibration signals or errors in the order analysis. Also these errors can be reduced or avoided at all.

The residual provided by the identification method, depends on the type of fault, the adequacy of the model and the accuracy of the experimental data. As some different faults can cause similar symptoms [8], the residuals associated with the actual fault can be not very lower than the residual of other possible but “wrong” faults.

Therefore, a lack of accuracy in the residual evaluation can cause a wrong identification of fault severity, of fault localisation and also of type of fault. This paper shows some methods that have been developed to measure the accuracy of the results obtained with model based techniques aimed to identify faults in rotating machines. The information provided by these methods can be very useful to evaluate which of the identified faults has the highest probability to be the actual one. Moreover, they can give important information about the adequacy of the model. For instance, these measures of accuracy can indicate probable errors in the stiffness and damping coefficients of a bearing, or in the experimental data as also a sensor failure.

The results of some first investigations on the capabilities of these methods are shown, which are carried out using both simulated data and experimental data of a real machine. The simulated responses have been used in order to give a complete overview on the sensitivity and the capability of the developed methods, which is not possible with the analysis of a single case study. The latter, instead, shows a successful use of the indexes, both on the identification of the correct fault type and on the model accuracy.

2. MEASURES OF ACCURACY OF THE RESIDUALS

The identification technique is described in detail in [12]. For the purposes of the present paper it is necessary to recall few concepts only. Using harmonic balance on the system, for each n^{th} harmonic component, following equation holds:

$$\left[-(n\Omega)^2\mathbf{M} + i\,n\Omega\mathbf{D} + \mathbf{K}\right]\mathbf{X}_n = \mathbf{F}_{f_n}(\Omega) \tag{1}$$

where the force vector $\mathbf{F}_{fn}$ can be composed by several fault equivalent forces $\mathbf{F}_{fn}^{(1)}$, $\mathbf{F}_{fn}^{(2)}$,…, $\mathbf{F}_{fn}^{(m)}$:

$$\mathbf{F}_{f_n}(\Omega) = \sum_{i=1}^{m} \mathbf{F}_{f_n}^{(i)}(\Omega) \tag{2}$$

Introducing the system dynamic stiffness matrix for the speed Ω_j and for the n^{th} harmonic component, eq. (1) can be rewritten as:

$$\left[\mathbf{E}\left(n\Omega_j\right)\right]\ \mathbf{X}_n^{(j)} = \sum_{i=1}^{m} \mathbf{F}_{f_n}^{(i)}(\Omega_j) = \mathbf{F}_{f_n}(\Omega_j) \tag{3}$$

Eq. (3) corresponds actually to a measured vibration at a certain rotating speed.

As the identification procedure can be time consuming the experimental data (additional vibrations) collected for a limited number only of suitable rotating speeds of the machine are analysed. Sometimes, this strategy is necessary also to avoid an overabundance of repeated observations that could cause numerical problems or identification errors. Obviously, different selections of the rotating speeds, that is different subsets of experimental data, can give quite different results in the fault identification. For instance, if the model does not simulate the response of the system very well near the critical speeds, then the selection of vibration data measured in speed ranges near the resonances should be avoided. If vector $\mathbf{X}_n$ indicates the vibrations corresponding to all the q rotating speeds of the considered speed transient, then vector Ξ_n indicates the measures, corresponding to a subset of p rotating speeds grouped in vector $\vec{\Omega}$, used for the identification procedure:

$$\vec{\Omega} = \left[\Omega_1\ \ \Omega_2\ \ \cdots\ \ \Omega_p\right]^{\mathrm{T}}, \quad \Xi_n = \left[\mathbf{X}_n^{(1)}\ \ \mathbf{X}_n^{(2)}\ \ \cdots\ \ \mathbf{X}_n^{(p)}\right]^{\mathrm{T}} \quad \text{with } p \le q \tag{4}$$

The expansion of eq. (3) gives:

$$\left[\mathbf{E}\left(n\vec{\Omega}\right)\right]\ \Xi_n = \begin{bmatrix} \mathbf{E}\left(n\Omega_1\right) & 0 & 0 & 0 \\ 0 & \mathbf{E}\left(n\Omega_2\right) & 0 & 0 \\ \vdots & \vdots & \vdots & \vdots \\ 0 & 0 & 0 & \mathbf{E}\left(n\Omega_p\right) \end{bmatrix} \begin{bmatrix} \mathbf{X}_n \\ \mathbf{X}_n \\ \vdots \\ \mathbf{X}_n \end{bmatrix} = \begin{bmatrix} \sum_{i=1}^{m} \mathbf{F}_{f_n}^{(i)}(\Omega_1) \\ \sum_{i=1}^{m} \mathbf{F}_{f_n}^{(i)}(\Omega_2) \\ \vdots \\ \sum_{i=1}^{m} \mathbf{F}_{f_n}^{(i)}(\Omega_p) \end{bmatrix} = \mathbf{F}_{f_n}(\vec{\Omega}) \tag{5}$$

and the vibration amplitudes can be obtained, defining the inverse of the elasto-dynamic matrix $\left[\mathbf{E}\left(n\vec{\Omega}\right)\right]$ as $\alpha_n(\vec{\Omega})\cdot\mathbf{F}_{f_n}(\vec{\Omega})$:

$$\Xi_n = \left[\mathbf{E}\left(n\vec{\Omega}\right)\right]^{-1}\cdot\mathbf{F}_{f_n}(\vec{\Omega}) = \alpha_n(\vec{\Omega})\cdot\mathbf{F}_{f_n}(\vec{\Omega}) \tag{6}$$

The lines in eq. (6) are rearranged, by partitioning the inverse of the system dynamic stiffness matrix, and omitting from α_n and $\mathbf{F}_{f_n}$ the possible dependence on $\vec{\Omega}$ for conciseness, in order to split the complex amplitude vector Ξ_{B_n}, corresponding to the d.o.f of the measured absolute vibrations in the measuring planes, from the vector Ξ_{A_n} of the remaining d.o.f. of the rotor system model:

$$\begin{cases} \Xi_{B_n} = \alpha_{B_n}\cdot\mathbf{F}_{f_n} \\ \Xi_{A_n} = \alpha_{A_n}\cdot\mathbf{F}_{f_n} \end{cases} \tag{7}$$

Using the first set of eqs. (7), it is possible to define, for each harmonic component, the vector differences $\vec{\delta}_n$, between calculated vibrations Ξ_{B_n} and measured vibrations Ξ_{ex_n}:

$$\vec{\delta}_n = \Xi_{B_n} - \Xi_{ex_n} = \alpha_{B_n}\cdot\mathbf{F}_{f_n} - \Xi_{ex_n} \tag{8}$$

and the scalar difference, called *relative residual*, as the square root of the ratio of the squared $\vec{\delta}_n$, divided by the sum of the squared measured vibration amplitudes Ξ_{ex_n}:

$$\delta_{r_n} = \left(\frac{\left[\alpha_{B_n} \cdot \mathbf{F}_{f_n} - \Xi_{ex_n} \right]^{*\mathrm{T}} \left[\alpha_{B_n} \cdot \mathbf{F}_{f_n} - \Xi_{ex_n} \right]}{\Xi_{ex_n}^{*\mathrm{T}} \Xi_{ex_n}} \right)^{1/2} \tag{9}$$

By means of the hypothesis of localisation of the fault along the rotor, the residual is calculated for each possible node of application of each fault. Therefore, δ_{r_n} is actually a surface in a $\square^{m+1}$ space. A least square approach is used in order to find the solution (identified faults) that minimize the differences which are calculated for all the different rotating speeds which are taken into consideration. The solution corresponds to the minimum of δ_{r_n}. A weighted last square identification is actually used, even if the analytical details are not reported here for conciseness. It is important to remark that the identified fault $\tilde{\mathbf{F}}_{f_n}$, that corresponds to the location and the amplitude/phase of the probable fault, i.e. the minimum value of δ_{r_n}, is function of the:

- used subset of the rotating speeds among those available at which the additional vibration considered;
- considered d.o.f.s, i.e. which are the measuring planes taken into account and the corresponding weights.

The proposed accuracy indexes can be grouped in three classes:

- global indexes;
- partial indexes;
- correlation indexes.

The indexes of the first and the second group derive from eq. (9). If the residuals are computed considering the errors evaluated at different d.o.f.s and at different machine rotating speeds, then they are called *global indexes*. On the contrary, those of the second group can be obtained by

selecting the vibration data evaluated at each single rotating speed or at each single d.o.f. and are called *partial indexes*.

2.1. GLOBAL INDEXES

By considering an harmonic component at once, the first index introduced, ε_1, is actually the minimum of eq. (9). However, if we consider that the result of the identification procedure is the equivalent force system $\tilde{\mathbf{F}}_f$ that represents the developing fault(s), the term $\alpha_B \cdot \tilde{\mathbf{F}}_f$ is the theoretical response $\Xi_{th}\big|_{\tilde{\mathbf{F}}_f}$ of the model to the identified fault(s) calculated for the rotating speed subset $\vec{\Omega}$ and for all the measured d.o.f.s. In other terms, we have:

$$\varepsilon_1 = \sqrt{\frac{\left(\Xi_{th}\big|_{\tilde{\mathbf{F}}_f} - \Xi_{ex}\right)^{*\mathrm{T}} \left(\Xi_{th}\big|_{\tilde{\mathbf{F}}_f} - \Xi_{ex}\right)}{\Xi_{ex}^{*\mathrm{T}} \cdot \Xi_{ex}}} \tag{10}$$

where the number of the elements of the vectors is equal to *p*. The dots on the experimental and theoretical curves shown in Figure 1 represent the values used to calculate ε_1.

Anyhow, the excitations obtained with the identification procedure can be used to evaluate the theoretical system response $\mathbf{X}_{th}\big|_{\tilde{\mathbf{F}}_f}$ at all the rotating speed associated with the experimental data. This allows a further residual estimation, ε_2, to be evaluated (see Figure 1), whose definition is formally equal to eq. (10), but the number of the elements of the vectors is equal to *q*:

$$\varepsilon_2 = \sqrt{\frac{\left(\mathbf{X}_{th}\big|_{\tilde{\mathbf{F}}_f} - \mathbf{X}_{ex}\right)^{*\mathrm{T}} \left(\mathbf{X}_{th}\big|_{\tilde{\mathbf{F}}_f} - \mathbf{X}_{ex}\right)}{\mathbf{X}_{ex}^{*\mathrm{T}} \cdot \mathbf{X}_{ex}}} \tag{11}$$

Sometimes, depending on the choice of the data used for the fault identification, although a very low value of the residual ε_1 is obtained, the residual estimation ε_2 could be significantly higher. This

is a symptom of a poor accuracy of the fault identification, as shown in case of Figure 1. This can be the consequence of a wrong selection of the type of fault as well as of a poor adequacy of the model. Further indexes allow the above mentioned causes of very different values of the residuals ε_1 and ε_2 to be discriminated. As the object of a fault diagnosis is to identify the actual machine malfunction as well as to simulate the system response, it is important to obtain a low value of both the residuals ε_1 and ε_2.

2.2. PARTIAL INDEXES

Both the residuals ε_1 and ε_2 are computed considering the errors evaluated at different d.o.f.s (those corresponding to the measuring planes) and at different machine rotating speeds. Therefore, they can be called global residuals and have also the property of being a number. On the contrary, further residual estimates can be obtained by selecting the vibration data evaluated at each single rotating speed Ω (see Figure 2) or at each single d.o.f. ξ (see Figure 3). These residual estimates can be denoted with ε_ω and ε_{dof} respectively:

$$\varepsilon_{\omega}(\Omega) = \sqrt{\frac{\left(\Xi_{th}(\Omega)\big|_{\tilde{\mathbf{F}}_f} - \Xi_{ex}(\Omega)\right)^{*\mathrm{T}} \left(\Xi_{th}(\Omega)\big|_{\tilde{\mathbf{F}}_f} - \Xi_{ex}(\Omega)\right)}{\Xi_{ex}^{*\mathrm{T}}(\Omega)\cdot\Xi_{ex}(\Omega)}} \tag{12}$$

$$\varepsilon_{\text{dof}}(\xi) = \sqrt{\frac{\left(\mathbf{X}_{th}(\xi)\big|_{\tilde{\mathbf{F}}_f} - \mathbf{X}_{ex}(\xi)\right)^{*\mathrm{T}} \left(\mathbf{X}_{th}(\xi)\big|_{\tilde{\mathbf{F}}_f} - \mathbf{X}_{ex}(\xi)\right)}{\mathbf{X}_{ex}^{*\mathrm{T}}(\xi)\cdot\mathbf{X}_{ex}(\xi)}} \tag{13}$$

These residuals are not defined with a single value, but they are functions of variables, like the machine rotating speeds or the d.o.f. associated to the measuring points.

They can be very useful to show the dependence of the error on the rotating speed and the measurement point. An application of ε_ω is shown in [12], where it is used to check the rotating speed range in which a test-rig model is adequate.

In the case of an ideal identification of the fault, the residuals should be scarcely affected by the speed value and the d.o.f.s. Owing to this, the analysis of the curves of the residual ε_ω vs. the rotating speed, as well as the curve of ε_{dof} vs. the d.o.f.s, can give very important information on the accuracy of the identified fault and the adequacy of the model. In general, the ratios between the standard deviations $\sigma_{\varepsilon_\omega}$ and $\sigma_{\varepsilon_{\text{dof}}}$ of the residuals ε_ω and ε_{dof} and their respective mean values μ_{ε_ω} and $\mu_{\varepsilon_{\text{dof}}}$ represent good measures of the identification accuracy:

$$\varphi_{\varepsilon_\omega} = \frac{\sigma_{\varepsilon_\omega}}{\mu_{\varepsilon_\omega}} \tag{14}$$

$$\varphi_{\varepsilon_{\text{dof}}} = \frac{\sigma_{\varepsilon_{\text{dof}}}}{\mu_{\varepsilon_{\text{dof}}}} \tag{15}$$

Moreover, it is necessary to consider that the residuals ε_1 and ε_2 represent a normalised estimate of the error. Therefore, equal values of the error between theoretical and experimental data can cause very different values of the residual depending on the vibration level. Even not too high absolute errors associated with a large number of very low vibration data can cause the normalised global residuals to reach high values.

On the contrary, sometimes, it is unimportant to approximate very well the experimental response also in speed ranges inside which very low vibrations occur. Then, also the analysis of the absolute error curve E vs. the rotating speed can give useful information:

$$E(\Omega) = \left(\mathbf{X}_{th}(\Omega)\big|_{\tilde{\mathbf{F}}_f} - \mathbf{X}_{ex}(\Omega) \right)^{*\mathrm{T}} \left(\mathbf{X}_{th}(\Omega)\big|_{\tilde{\mathbf{F}}_f} - \mathbf{X}_{ex}(\Omega) \right) \tag{16}$$

2.3. CORRELATION INDEXES

Interesting results can be obtained by a correlation analysis between theoretical and experimental data. The real and imaginary parts of all the theoretical and the experimental vibrations can be located into the two real vectors $\widehat{\mathbf{X}}_{th}$ and $\widehat{\mathbf{X}}_{ex}$, respectively. Then, the Modal Scale Factor (MSF) and the index called Modal Assurance Criterion (MAC) [18], can be evaluated as follows:

$$\mathrm{MSF} = \frac{\widehat{\mathbf{X}}_{th}^{\mathrm{T}} \widehat{\mathbf{X}}_{ex}}{\widehat{\mathbf{X}}_{ex}^{\mathrm{T}} \widehat{\mathbf{X}}_{ex}} \tag{17}$$

$$\mathrm{MAC} = \frac{\left| \widehat{\mathbf{X}}_{ex}^{\mathrm{T}} \widehat{\mathbf{X}}_{th} \right|^2}{\left(\widehat{\mathbf{X}}_{ex}^{\mathrm{T}} \widehat{\mathbf{X}}_{ex} \right) \left(\widehat{\mathbf{X}}_{th}^{\mathrm{T}} \widehat{\mathbf{X}}_{th} \right)} \tag{18}$$

If $\widehat{\mathbf{X}}_{th}$ coincides with $\widehat{\mathbf{X}}_{ex}$ the value of the indexes MSF and MAC is 1. Anyhow, as the identification procedure is based on a least square method, in this application the MSF value is always very close to 1. That is, in order to obtain a null value of the mean error, under-estimations and over-estimations of the experimental data are compensated over the whole set of data. On the contrary, the MAC index gives a measure of the dispersion of the data from the straight line whose angular coefficient is the MSF value. In addition, a linear regression analysis of the data contained in the vectors $\widehat{\mathbf{X}}_{th}$ and $\widehat{\mathbf{X}}_{ex}$ can be carried out. The difference between the angular coefficient *m* of the regression line and the ideal unity value is a further measure of accuracy of the fault identification. In the end, an additional information is represented by the value of the standard deviation σ_r of the errors obtained with the linear regression analysis.

3. NUMERICAL APPLICATION

The validation of the method developed to measure the accuracy of the results of the identification technique has been carried out by simulating the experimental response of a rotor train composed of a high-intermediate pressure turbine (HP-IP) and a low pressure turbine (LP). Each rotor was supported on two oil-film journal bearings while a rigid foundation of the machine has been considered. Figure 4 shows the FE model of the rotors.

The supports have been numbered from #1 to #4. In order to simulate an ideal experimental response of the system due to a rotor bow, two equal but opposite moments have been applied to the ending nodes of a finite element of the mesh located near bearing #2 (Figure 4). The machine response has been evaluated in the range from 400 rpm to 3000 rpm. The first balance resonance of the HP-IP turbine was nearly 1550 rpm while the second critical speed was nearly 2900 rpm. Only the radial vibrations, in vertical and horizontal direction, evaluated at the four journal bearings have been considered for the fault identifications. These d.o.f.s have been numbered from one to eight, starting from bearing #1 to bearing #4.

The sensitivity of the measures of accuracy of the fault identification techniques has been studied by analysing the effects on the residual induced by the identification of wrong faults, by noised vibration signals as well as by mistuned models. The considered cases have been:

- Case 1: exact model, bending moments identification
- Case 2: exact model, unbalance identification (speeds in the range 1500-3000 rpm)
- Case 3: exact model, unbalance identification (speeds in the range 1150-2300 rpm)
- Case 4: exact model, noised signals, bending moments identification
- Case 5: corrupted model (brg. coeff. #1 and #2), bending moments identification
- Case 6: corrupted model (brg. coeff. #2), bending moments identification
- Case 7: corrupted model (brg. coeff. #2), unbalance identification

Some significant results are summarized in Table 1, while few cases are described in detail hereafter. A deeper analysis can be found in [19].

(Table 1 about here)

3.1. Case 1: Exact Model, Bending Moments Identification and Case 2: Exact Model, Unbalance Identification (Speeds in The Range 1500-3000 rpm)

In Case 1, the two bending moments used to simulate the experimental response have been correctly identified as proved by the results reported in Table 1 as well as by the Bode plots shown in Figure 5 and Figure 6.

In absence of non linear effects the harmonic content of the actual vibrations induced by a similar fault would show only a 1x rev. component (1X). This symptom is quite similar to that one caused by a rotor unbalance as regards the harmonic content. Therefore, an identification analysis has been carried out considering a lumped unbalance mass as machine fault (Case 2). Vibration data associated with seven rotating speeds equally spaced in the range from 1500 rpm to 3000 rpm have been used for the identification procedure. That is, no data has been selected in the range of low speeds, below the first balance resonance, in which an unbalance would excite much lower vibration amplitudes with respect to the values excited by the applied local bow. The curve of the relative residual, δ_r, evaluated for a single unbalance mass located at different sections of the HP-IP turbine is shown in Figure 7.

The identified unbalance has been used to obtain the evaluation of the residual ε_2.This residual (see Table 1) was not much higher than the minimum residual obtained with the identification procedure. Although the type of the identified fault was not correct, these residuals were rather low and fairly similar. Owing to this, an unbalance, instead of a bow, could be supposed to be the actual fault. However, some important and clear information can be obtained with the methods that have

been developed. Figure 8 shows the relationship between the residuals and the rotating speed. When the speed is lower than 1200 rpm the vibrations caused by the unbalance are significantly lower than those induced by the bow: this cause the residual to increase (see Figure 5 and Figure 6). This information indicates that a wrong fault has been identified.

Figure 9 shows the dependence of the residuals on the eight d.o.f. that have been considered. As the vibrations induced by the bending moments were rather low at the two bearings of the LP turbine, the residuals associated with the unbalance were higher at the d.o.f. 5÷8 in respect to those calculated for the d.o.f. 1÷4 of the supports of the HP-IP turbine. The absolute error between the machine responses due to the bow and the unbalance, respectively, increases with the rotating speed (Figure 10). This is a further indication that the identified fault is not correct. Figures 7 and 8 show the Bode plots of the 1X theoretical vibrations evaluated at bearings #2 and #3, in the horizontal direction, using the identified unbalance. These vibrations are compared with the simulated experimental response as well as with the response obtained with the bending moments identified using the exact model of the fully assembled machine.

3.2. CASE 5: CORRUPTED MODEL (BRG. COEFF. #1 AND #2), BENDING MOMENTS IDENTIFICATION

In order to simulate a not unusual lack of accuracy of the models, the stiffness and damping coefficients of the two bearings of the HP-IP turbine (brg. #1 and #2) have been multiplied by a scale factor of 0.5 in the rotating speed range from 400 rpm to 2000 rpm. The simulated response due to two opposite bending moments applied to the original exact model has been assumed as experimental response of the system while the two moments have been identified using the corrupted model whose bearing coefficients had been modified. Some results of this investigation are reported in Table 1.

The amplitude and the phase of the identified moments approximate the exact values very well, while the identified finite element of the model to which the bending moments are applied is adjacent to the right one and has the same mass and stiffness. Figure 11 shows the dependence of the residuals on the rotating speed. In the speed range from 1200 rpm to 1550 rpm the residuals are rather high and differ significantly from the mean value of the residuals evaluated over the complete speed range of the analysis. Figure 12 shows the Bode plot of the 1X vibrations evaluated at bearing #2, in the horizontal direction, using the identified moments. This response is compared with the simulated experimental response evaluated with the exact model. Owing to the considerable reduction of the oil-film stiffness coefficients the first balance resonance of the corrupted model of the HP-IP turbine decreases in respect to that one of the original model. Therefore, although the bending moments have been identified with a fairly good accuracy the differences between the responses obtained with the two models are consistent. This affects the values of the residuals significantly, especially in the speed range near the shaft critical speeds. This is emphasised also by the high ratio between the standard deviation of the residuals evaluated at different speeds and their mean value (Table 1).

4. EXPERIMENTAL RESULTS

In order to carry out a further validation of the methods developed for evaluating the accuracy of fault identifications, the experimental vibrations, in both horizontal and vertical directions, of the generator of a co-generation unit have been analysed. The coupling between generator and gas turbine was provided by a gearbox whose wheels were mounted on a quill-shaft. Figure 13 shows the finite element model of the generator. The rotor was supported on two fluid-film journal bearings (#1, #2) that were equipped with two radial XY proximity probes. Bearing #2 was mounted at the driven end of the generator, beyond the flange of the rigid coupling, that is on a gear shaft.

Owing to the flexibility of the quill-shaft, the influence of the gear shafts on the dynamic behaviour of the generator has been neglected: therefore, only the generator and a portion of a gear shaft have been modelled.

Figure 14 shows the Bode plot of the synchronous vibrations (1X) measured on bearing #1, in vertical direction, during a rundown (Case A) and two run-ups (Cases B and C). The curves both of amplitude and phase show significant differences in the machine behaviour occurred during the three transients, especially in the speed range near the first balance resonance of the rotor (1740 rpm). The second run-up (Case C) was carried out at the end of a two day's downtime without a suitable rotor straightening on the turning gear. On the contrary, the first run-up (Case B) occurred with straightened rotor after a very short downtime period, during which the machine was operated in barring mode. During the transients A and C, the generator was supposed to be affected by a shaft bow. However the causes of these bows are different in the two cases.

4.1. Extended Bow Identification

In the operating condition the 1X vibrations of the generator showed to be influenced by the value of the exciter current. Therefore it was supposed that the rotor was subjected to a bow induced by unsymmetrical axial forces caused, for instance, by an excessive or an unsymmetrical thermal expansion of the copper bars mounted inside the generator slots. Conversely, when the operating time on turning gear is too short to cause a complete straightening of the generator rotor, high vibrations occur during the runups, especially when approaching the first balance resonance. In the following, the identification of the machine malfunction has been carried out considering only the additional vibrations evaluated on the basis of the transients A and B, that is a rundown and a subsequent runup carried out with a straightened rotor.

A rotor bow can be simulated by applying two opposite bending moments, having the same amplitude, to suitable nodes of the FE model of the rotor. The middle part of the generator rotor, where the copper bars are mounted, has been modelled with an even number of finite elements, equal to six, so that a node (no. 13) was located in the mid-span of the rotor windings (Figure 13 and Figure 15). These six elements were symmetrical with respect to the central node (no. 13). If the fault was really a rotor bow induced by thermal effects in the windings it was rather probable that the two equivalent bending moments should have been applied to the ends of the windings, or near the retaining rings, in rotor sections symmetrical in respect to the mid-span of the windings.

When the fault is modelled with two opposite moments the identification of the minimum residual is obtained by considering groups of different numbers of adjacent finite elements whose extreme nodes are the points to which the bending moments are applied. Obviously, also the mean position of each group of FE is changed along the rotor. The minimum residual obtained with a complete analysis gives the best estimate of location and amplitude of the moments. Then, this residual can be compared with those evaluated by considering other types of faults in order to evaluate the most probable fault.

Vibration data associated with ten rotating speeds equally spaced in the range from 800 rpm to 2800 rpm have been used to identify the two bending moments.

During the identification procedure, bending moments have been applied to groups of 2, 4 and 6 adjacent finite elements. For each number of elements the minimum residual corresponded to a group of FE centred around the node no. 13, that is a node located in the mid-span of the rotor windings. The values of the minimum residuals are shown in Table 2. Although the differences between these residuals are very little, the minimum residual is that one associated with a group of four elements, whose mean position is just in the mid-span of the rotor windings while the nodes to which the bending moments are applied are not exactly at the extremes of the windings but,

anyhow, in their vicinity (nodes 11 and 15). Figure 15 shows the dependence of the relative residual on the position of two opposite bending moments applied at the extreme nodes of different groups of four adjacent finite elements.

(Table 2 about here)

Figure 16 and Figure 17 show the Bode plots of the 1X vibrations evaluated with the model on bearings #1 and #2 using the identified bending moments, compared with the respective experimental one. With regard to the vertical vibrations, the numerical response on both the bearings are in good accordance with the experimental behaviour, while the error in the horizontal direction is not negligible, especially in the range around the balance resonance. Concerning this, it is important to consider that on both the bearings, when passing through the first balance resonance, the 1X vertical vibrations were up to three times higher than the horizontal vibrations. In addition to this, the horizontal additional vibrations do not show a significant and evident positive peak in the speed range near the first balance resonance of the generator. This abnormal behaviour can be induced by a machine misalignment as well as by the bearing characteristics. In order to simulate this behaviour with care a preliminary tuning of the model has been carried out, however, a further optimisation of some bearing coefficient would be required. Anyhow, the identified bending moments allow the highest vibrations to be simulated with a good accuracy over the complete speed range from 800 rpm to 2800 rpm.

4.2. USE OF FAULT IDENTIFICATION MEASURES OF ACCURACY

The calculation of ε_2 has been carried out by considering the identified moments and all the available vibrations data associated with 68 rotating speed values almost uniformly spaced in the range from 800 rpm to 2800 rpm (Table 2). The values of the residuals ε_1 and ε_2 are very similar although they have been obtained using a quite different number of vibration data. Therefore the

fault identification was not significantly influenced by a “biased” choice of the vibration data. The residuals ε_1 and ε_2 are not very low and the analysis of the residuals ε_{dof} shows that the residuals associated with the vertical vibrations are rather low and they are significantly lower than the residuals associated with the horizontal vibrations (Figure 18).

The four residuals ε_{dof} summarise the results obtained by the comparison between the experimental and the numerical responses shown in Figure 16 and Figure 17. Figure 19 shows the dependence of the residuals ε_ω on the rotating speed. At first, both vertical and horizontal vibrations on the two bearings have been considered (case: 4 dof). The bold line in Figure 19 shows that in the speed range below the first balance resonance the residuals are rather high while in the range above 1700 rpm they decrease significantly up to a mean value of about 0.6. This behaviour can be ascribed, mainly, to errors in the evaluation of some bearing coefficient, mostly in the horizontal direction.

Since in this case vertical vibrations were more significant, residual ε_ω, which takes into account only two d.o.f.s, is shown by the thin line shown in Figure 19 (case: 2 dof). Contrary many usual results, the curve of this residual shows a quite evident negative peak just in the speed range around the first critical speed of the generator. The low values of the residuals inside this speed range are a clear indication of the accuracy of the fault identification.

The residuals obtained with this analysis increase in the ranges below and above the critical speed only because of the low amplitudes of the additional vibrations that occurred outside the resonance peak. In fact, as shown by eq. (9), the residual is a relative estimate of the error. The dependence of the absolute error on the rotating speed is shown in Figure 20. If only the vertical vibrations are considered (case: 2 d.o.f., thin line), the absolute error is nearly constant over the complete speed range from 800 rpm to 2800 rpm. This cause the relative error ε_ω to increase when the vibration amplitudes decrease significantly.

Moreover, it is necessary to consider that the additional vibrations should be caused only by the fault that must be identified. Therefore, the two speed transients used to evaluate the additional vibrations must be chosen with care, however, when the amplitude of the additional vibrations is rather low, the error in the phase evaluation can be important because these low vibrations can be due also to other secondary unexpected causes.

Figure 21 shows the results of a regression analysis carried out between experimental and numerical vibration data. In accordance with the results above described the larger dispersion of the data is associated with the vibrations that show the lowest levels. The estimates of the MAC index as well as some results of a statistical analysis of the residuals ε_ω, obtained with the identified moments, are reported in Table 3.

(Table 3 about here)

4.3. UNBALANCE (FALSE FAULT) IDENTIFICATION

In this case study, the fault has occurred on a generator and not on a turbine; this fact as well as some significant symptoms suggested that the fault was a rotor bow. Anyhow, in order to evaluate the capabilities of the techniques developed, a further investigation has been carried out considering a local unbalance as the cause of the additional vibrations of the generator.

The identification of position and magnitude of the equivalent force due to a rotor unbalance has been obtained with the same sub-set of vibration data previously used to identify the bending moments. Figure 15 shows the dependence of the relative residual on the axial position of the unbalance.

The minimum residual obtained with this analysis has been evaluated by applying a local unbalance to the node no. 13, that is the node located in the mid-span of the rotor windings. Afterwards, the identified unbalance has been used to evaluate the residual ε_2, obtained considering all the available

vibration data. The values of the two residuals ε_1 and ε_2 were very similar (ε_1 = 1.1463, ε_2 = 1.0779), but they are significantly higher than the respective residuals obtained with the identification of the rotor bow (Table 2).

Figure 22 shows the Bode plot of the 1X vibrations evaluated with the model on bearings #1 using the identified unbalance. In the same figure, the numerical response of the system has been compared with the respective experimental one similar results are obtained on bearing #2. Figure 22 shows that even the best identified local unbalance cause significant errors over the complete speed range from 800 rpm to 2800 rpm, not only in the range outside the region of the resonance peak.

Figure 23 shows the curves both of the relative ε_ω and the absolute errors vs. the generator rotating speed. These curves, which have been obtained considering both vertical and horizontal vibrations, can be compared with the respective ones shown in Figure 19 and Figure 20 (case: 4 dof). In general, the absolute and the relative errors associated with the identified unbalance are higher than the errors associated with the rotor bow.

By considering the characteristics of the machine and the fault symptoms, the type of the identified fault and the position of the equivalent bending moments along the rotor can considered highly probable. Although the results of the fault identification are rather good, a further refining of the tuning of the bearing coefficients could probably allow a more accurate identification of the moments to be obtained.

5. CONCLUSIONS

In the paper, the capabilities of some different methods developed to measure the accuracy of the results obtained with model based techniques aimed to identify faults in rotating machines are shown. A poor accuracy of the results of the fault identification can be caused by a wrong selection of the type of fault, by a poor adequacy of the model of the fully assembled machine as well as by

the presence of noise in the vibration signals. The results described in the paper have shown that all these causes that affect the accuracy of the identification results can be detected. First simulated responses have been used and this investigation has allowed a useful sensitivity analysis of the developed methods to be carried out. Then the developed methods have been successfully used also for the analysis of experimental vibrations of a real machine.

These proposed diagnostic techniques have shown to be able to give useful information for identifying the most probable fault also when different sets of equivalent excitations, which can induce fault symptoms very similar to the real one, are considered. Therefore, these methods are helpful to discriminate the actual fault from other wrong but probable faults. In addition to this, these methods have shown to be very useful to detect lacks of accuracy in the model of the fully assembled machine (for instance probable errors in the stiffness and damping coefficients of a bearing) as well as errors in the experimental vibration data or a sensor failure.

REFERENCES

1. R. Isermann and M. Ulieru 1993 Systems, Man and Cybernetics 1, 743-748. Integrated Fault Detection and Diagnosis.
2. R. Isermann 1997 Control Engineering Practice 5(5), 639-652. Supervision, Fault-detection and Fault-diagnosis Methods – An Introduction.
3. M.F. White and M. Jecmenica 1999 COMADEM 99 Sunderland UK July 1999. Fault Diagnosis Using a Fault Matrix Incorporating Fuzzy Logic.
4. N.S. Vyas and D. Satishkumar 2001 Mechanism and Machine Theory 36(2), 157-175. Artificial Neural Network Design for Fault Identification in Rotor-bearing System.

5. A. Lucifredi, C. Mazzieri and M. Rossi 2000 Mechanical System and Signal Processing 14(3), 471-494. Application of Multiregressive Linear Models, Dynamic Kriging Models and Neural Network Models to Predictive Maintenance of Hydroelectric Power Systems.
6. R. Isermann and P. Ballé 1997 Control Engineering Practice 5(5), 709-719. Trends in the Application of Model-based Fault Detection and Diagnosis of Technical Process.
7. N. Bachschmid, A. Vania, E. Tanzi, and P. Pennacchi 1999 EURO DINAME 99 Günzburg Germany July 1999, 3-11. Identification and Simulation of Faults in Rotor Systems: Experimental Results.
8. N. Bachschmid and P. Pennacchi 2000 7th Int. Conf. On Vibrations in Rotating Machinery IMechE Nottingham UK September 2000, 571-580. Model Based Malfunction Identification from Bearing Measurements.
9. N. Bachschmid, P. Pennacchi, E. Tanzi and A. Vania 2000 Journal of the Brazilian Society of Mechanical Sciences XXII(3), 423-442. Accuracy of Modelling and Identification of Malfunctions in Rotor Systems: Experimental Results.
10. D-H. Hellmann 2002 ISROMAC 9 Honolulu Hawaii February 2002, 1-5. Early Fault Detection – An Overview –
11. R.J. Patton, S. Simani, S Daley and A. Pike 2001 Surveillance Compiègne France October 2001, 27-48. Identification and model-based fault diagnosis of a gas turbine system.
12. N. Bachschmid, P. Pennacchi and A. Vania, 2002 Journal of Sound and Vibration 254(2), 327-366. Identification of Multiple Faults in Rotor Systems.
13. R. Isermann 1995 Surveillance 2 Senlis France October 1995, 777-792. Fault Detection and Diagnosis - Methods and Applications -.
14. R. Markert, R. Platz and M. Seidler 2000 ISROMAC-8, 901-907. Model Based Fault Identification in Rotor Systems by Least Squares Fitting.

15. R. Platz, R. Markert and M. Seidler 2000 7th Int. Conf. On Vibrations in Rotating Machinery, IMechE Nottingham UK September 2000, 581-590. Validation of Online Diagnostics of Malfunctions in Rotor Systems.
16. R. Platz and R. Markert 2001 Surveillance Compiègne France October 2001, 435-446. Fault models for on-line identification of malfunctions in rotor systems.
17. N. Bachschmid, P. Pennacchi, A. Vania, G.A. Zanetta and L. Gregori 2002 ISROMAC 9 Honolulu Hawaii February 2002, 1-11. Identification of Rub and Unbalance in a 320MW Turbogenerator.
18. D.J. Ewins 1984 Modal Testing: Theory and Practice, Letchworth: Research Studies Press.
19. P. Pennacchi and A. Vania 2001 AIMETA XV Taormina Italy September 2001, 1-12. Measures of Accuracy of Model Based Identification of Faults in Rotormachinery.

ACKNOWLEDGEMENTS

This work is partially funded by the MIUR (Italian Ministry for the University and Scientific Research) Cofinanziamento "TECNICHE DI IDENTIFICAZIONE DI MALFUNZIONAMENTI DI SISTEMI MECCANICI BASATE SULL'ANALISI DEL COMPORTAMENTO DINAMICO" for the year 2001.

Table 1 Case 1: Exact Model, Bending Moment Identification

	ε_1	ε_2	μ_{ε_ω}	$\sigma_{\varepsilon_\omega}$	$\varphi_{\varepsilon_\omega}$	$\mu_{\varepsilon_{\mathrm{dof}}}$	$\sigma_{\varepsilon_{\mathrm{dof}}}$	$\varphi_{\varepsilon_{\mathrm{dof}}}$	m	σ_r [μm]	MAC	M (ampl.)	M phase
Case 1	0.612e–3	0.632e–3	0.596e–3	0.107e–6	0.179e–5	0.631e–3	0.350e–4	0.555e–1	1.0003	0.02	0.9996	8.006e5	–89.9°
Case 2	0.3292	0.4136	0.5387	0.2224	0.4128	0.6531	0.2857	0.4374	1.1340	16.53	0.7878	–	–
Case 3	0.4049	0.7240	0.6337	0.2661	0.4199	0.2890	0.8488	2.9370	1.3350	25.77	0.6085	–	–
Case 4	0.0816	0.0771	0.1045	0.0604	0.5780	0.1072	0.1216	1.1343	0.9648	3.14	1.0313	7.767e5	–90.5°
Case 5	0.5772	0.5814	0.5804	0.1946	0.3352	0.6001	0.1746	0.2909	1.0477	23.4	0.7312	8.006e5	–95.2°
Case 6	0.3109	0.3116	0.3373	0.0663	0.1965	0.3857	0.1072	0.2779	0.7747	12.62	1.1925	5.475e5	–75.3°
Case 7	0.4193	0.4854	0.6308	0.2088	0.3310	0.7408	0.3103	0.4188	0.7472	19.43	1.019	–	–

Exact bending moment value: M = 8.000e5 [Nm], phase = –90°

Table 2 Measures of accuracy of the fault identification

	Number of finite elements		
	6	4	2
Extreme nodes	10 / 16	11 / 15	12 / 14
Residual ε_1	0.8346	0.8107	0.8135
Residual ε_2	0.8440	0.8273	0.8290
MAC	0.6635	0.6992	0.6956

Table 3 Measures of accuracy of the fault identification

Degrees of freedom	Residual ε_1	Residual ε_ω Mean value	Residual ε_ω Standard dev. σ_ω	MAC
4 d.o.f.	0.8273	0.7917	0.1725	0.6992
2 d.o.f.	0.3647	0.6508	0.2457	0.9401

FIGURE CAPTIONS

Figure 1 Choice of the vibration data used to evaluate indexes $\varepsilon 1$ (left) and $\varepsilon 2$ (right).

Figure 2 Calculation of index ε_{ω}.

Figure 3 Calculation of index ε_{dof}.

Figure 4 Finite Element Model of the rotor train.

Figure 5 Bode plot of 1X vibrations at brg. #2. Exp.: experimental data. Cases 1 and 2: theoretical response.

Figure 6 Bode plot of 1X vibrations at brg. #3. Exp.: experimental data. Cases 1 and 2: theoretical response.

Figure 7 Unbalance identification.

Figure 8 Dependence of residuals on rotating speed: unbalance identifications.

Figure 9 Dependence of residuals on d.o.f.s.

Figure 10 Absolute error $E(\Omega)$ vs. rotating speed.

Figure 11 Dependence of residuals on rotating speed (Case 5).

Figure 12 Bode plot of experimental and theoretical (Case 5) vibrations at brg. #2, horizontal direction.

Figure 13 Finite Element model of the generator rotor.

Figure 14 Bode plot of 1X transient vibrations measured on bearing #1, in vertical direction, during different speed transients (Case A: rundown, Cases B and C: runups).

Figure 15 Dependence of the relative residual on the axial position of the two bending moments and on the position of the local unbalance.

Figure 16 Comparison between the experimental 1X vibrations measured on bearing #1 and the respective numerical response obtained with the identified bending moments.

Figure 17 Comparison between the experimental 1X vibrations measured on bearing #2 and the respective numerical response obtained with the identified bending moments.

Figure 18 Dependence of the residuals, ε_{dof}, on the degree of freedom.

Figure 19 Dependence of the residuals, ε_{ω}, on rotating speed.

Figure 20 Absolute error vs. rotating speed.

Figure 21 Regression analysis.

Figure 22 Comparison between the experimental 1X vibrations measured on bearing #1 and the respective numerical response obtained with the identified unbalance.

Figure 23 Relative and the absolute errors vs. the generator rotating speed.

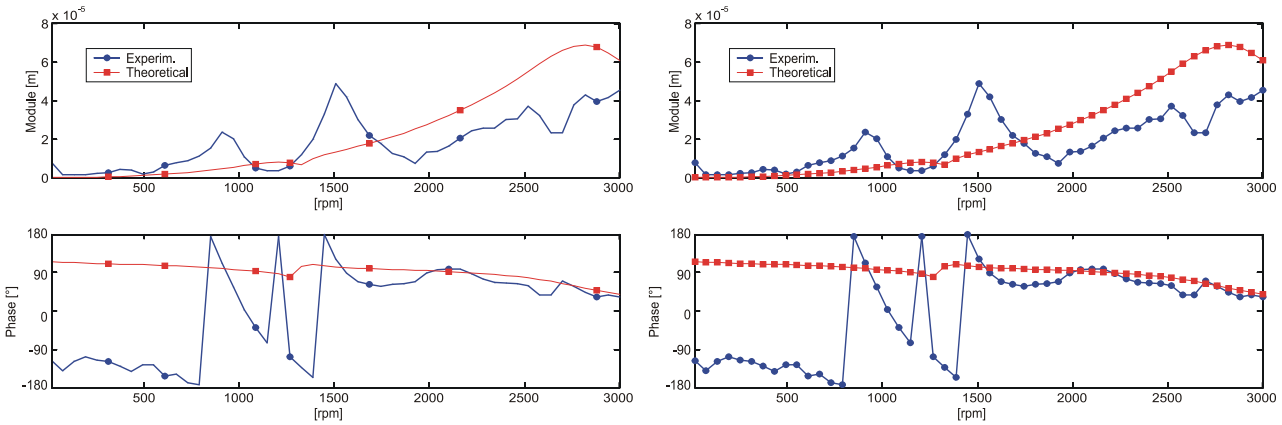

Figure 1 Choice of the vibration data used to evaluate indexes ε_1 (left) and ε_2 (right).

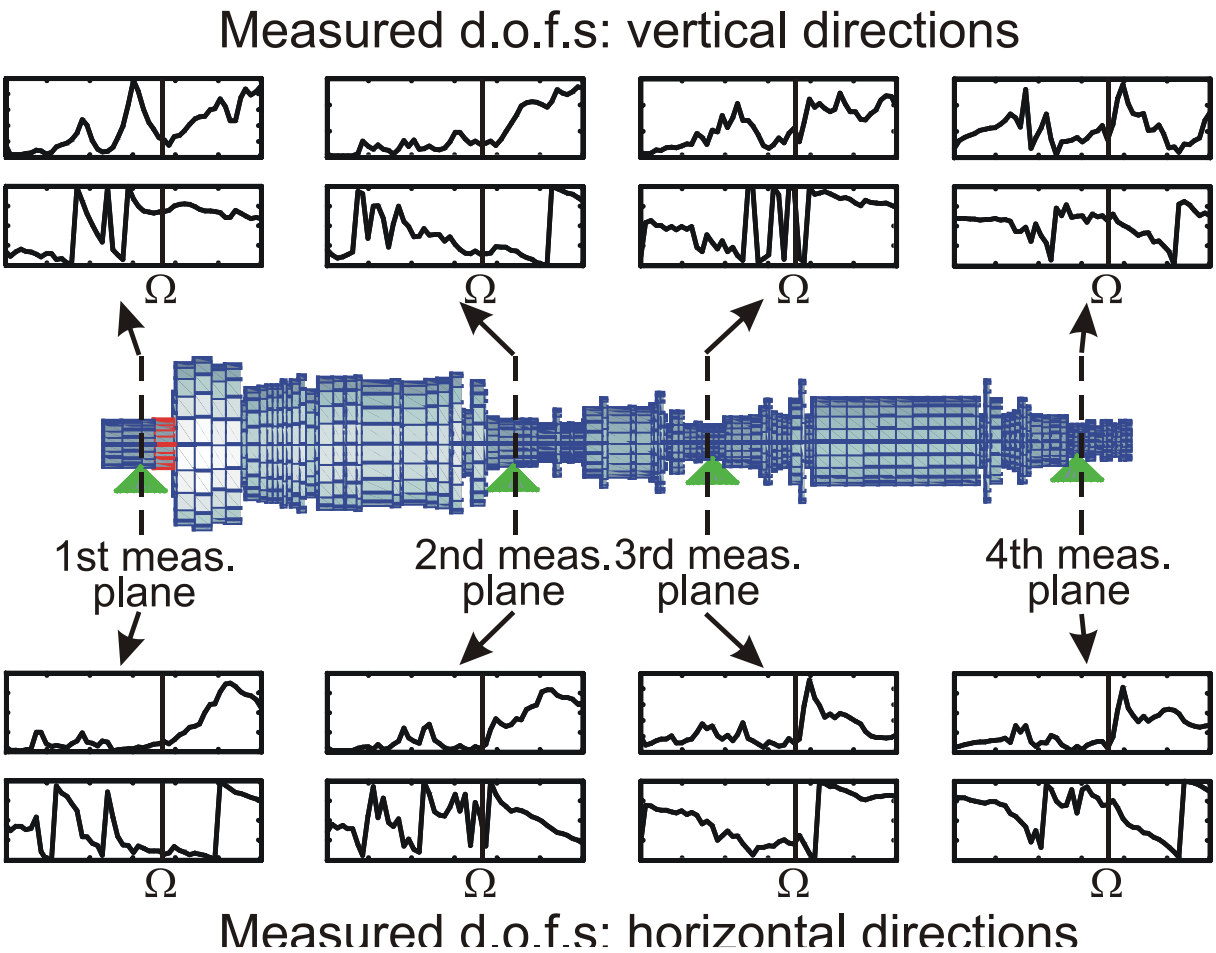

Figure 2 Calculation of index ε_{ω}.

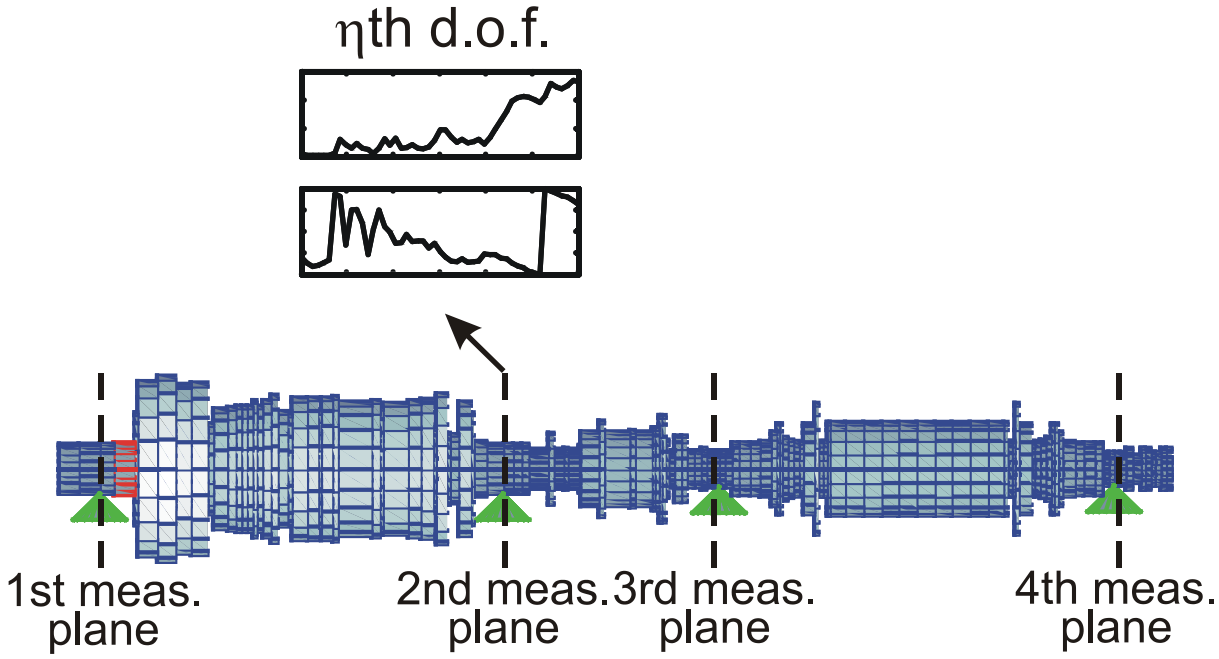

Figure 3 Calculation of index ε_{dof}.

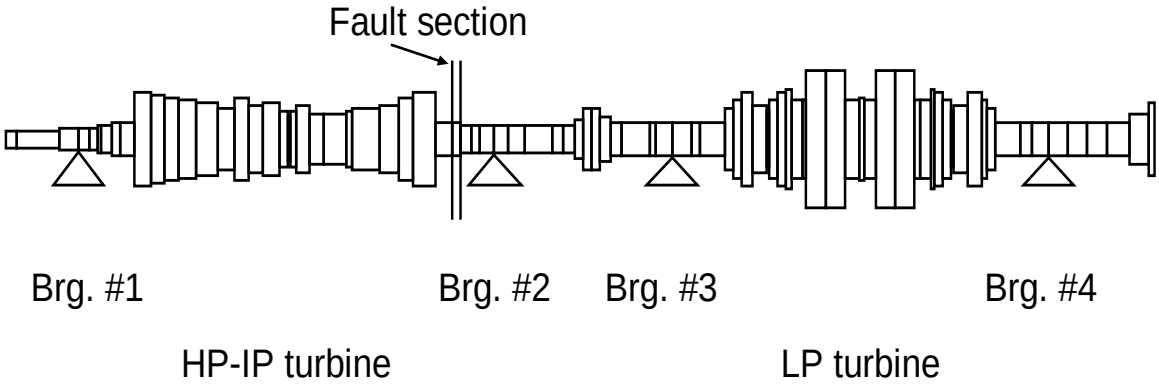

Figure 4 Finite Element Model of the rotor train.

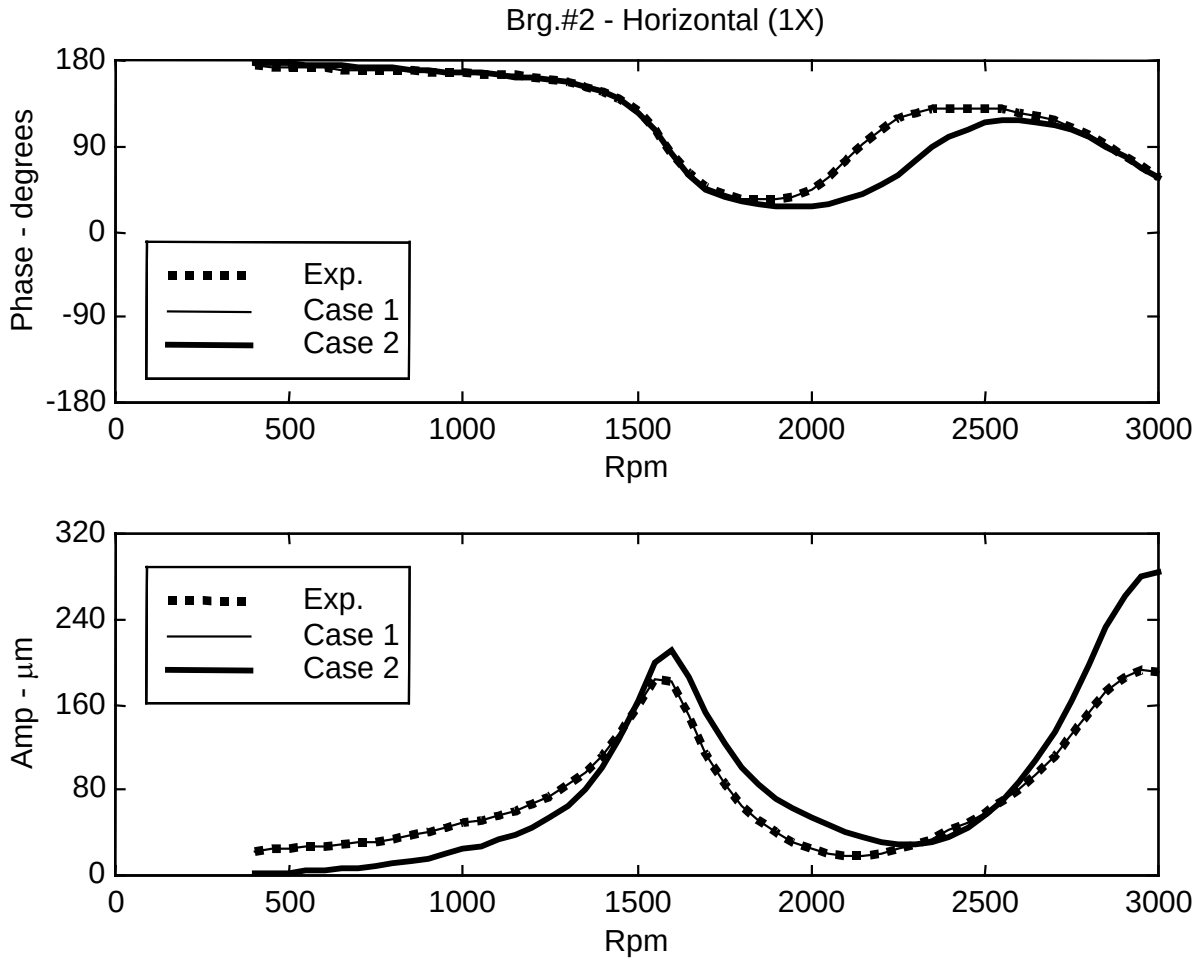

Figure 5 Bode plot of 1X vibrations at brg. #2. Exp.: experimental data. Cases 1 and 2: theoretical response.

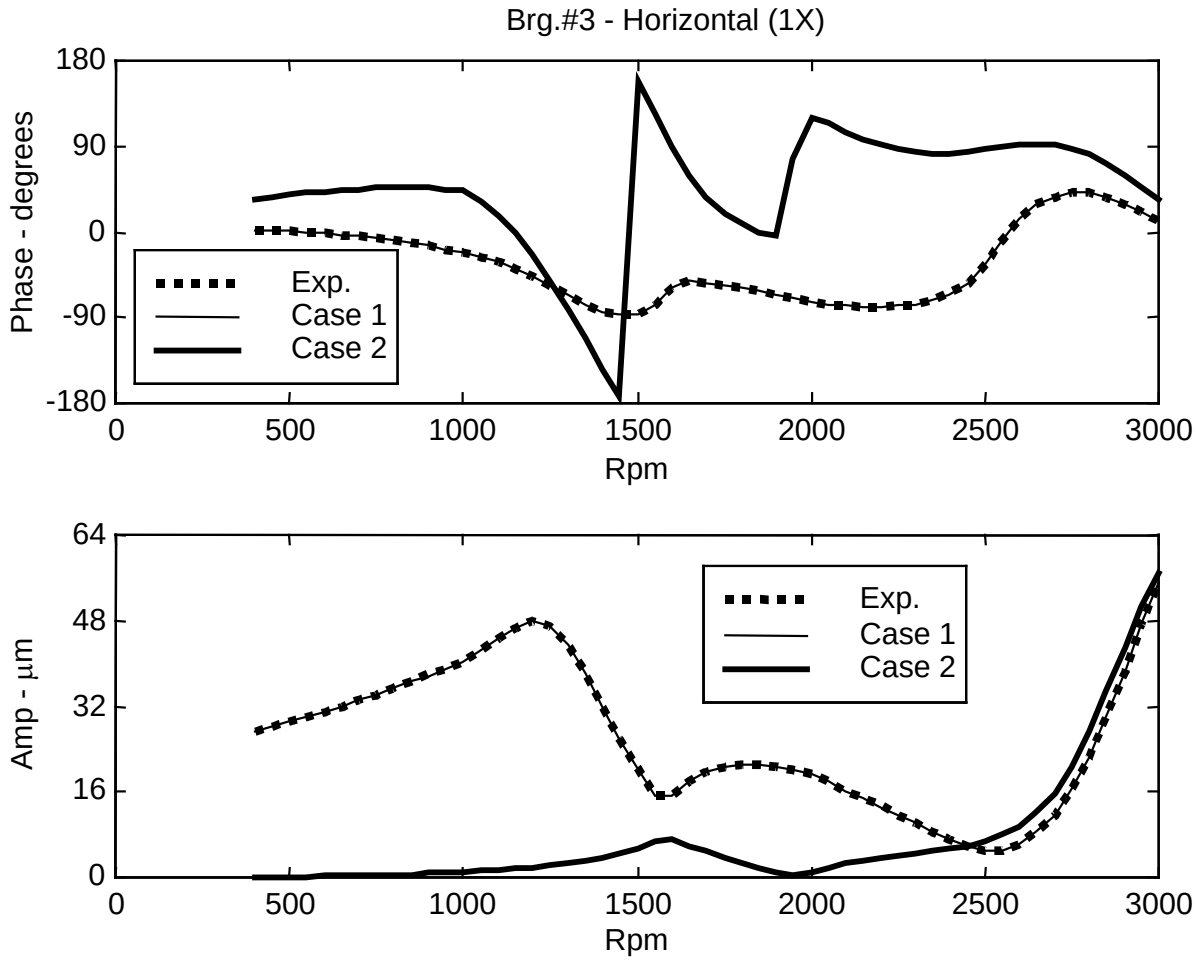

Figure 6 Bode plot of 1X vibrations at brg. #3. Exp.: experimental data. Cases 1 and 2: theoretical response.

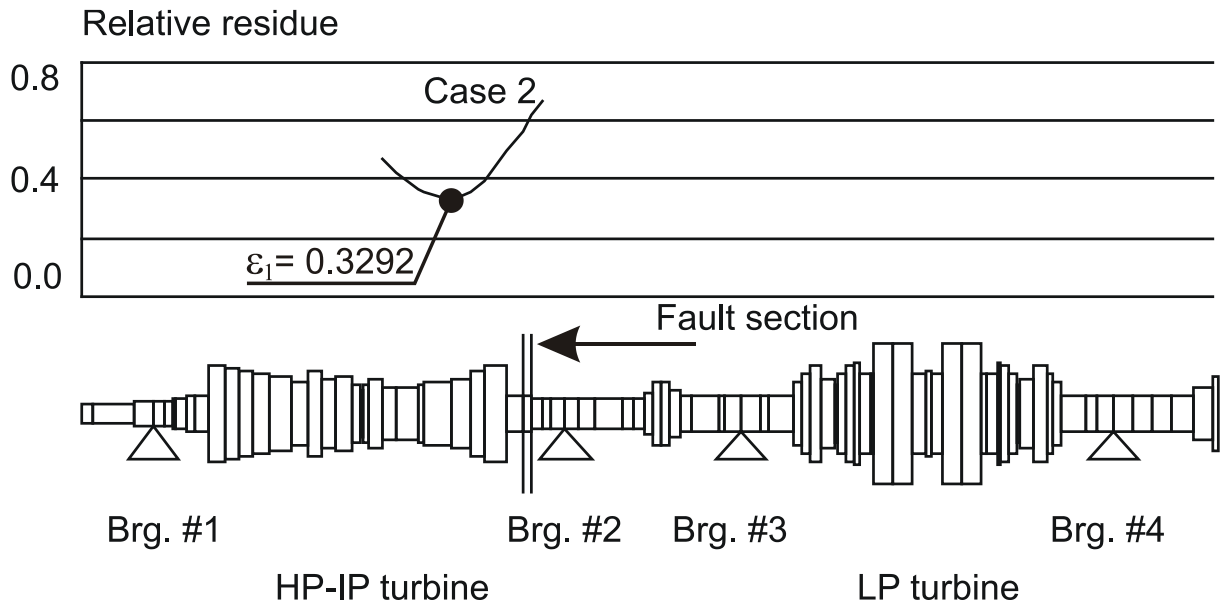

Figure 7 Unbalance identification.

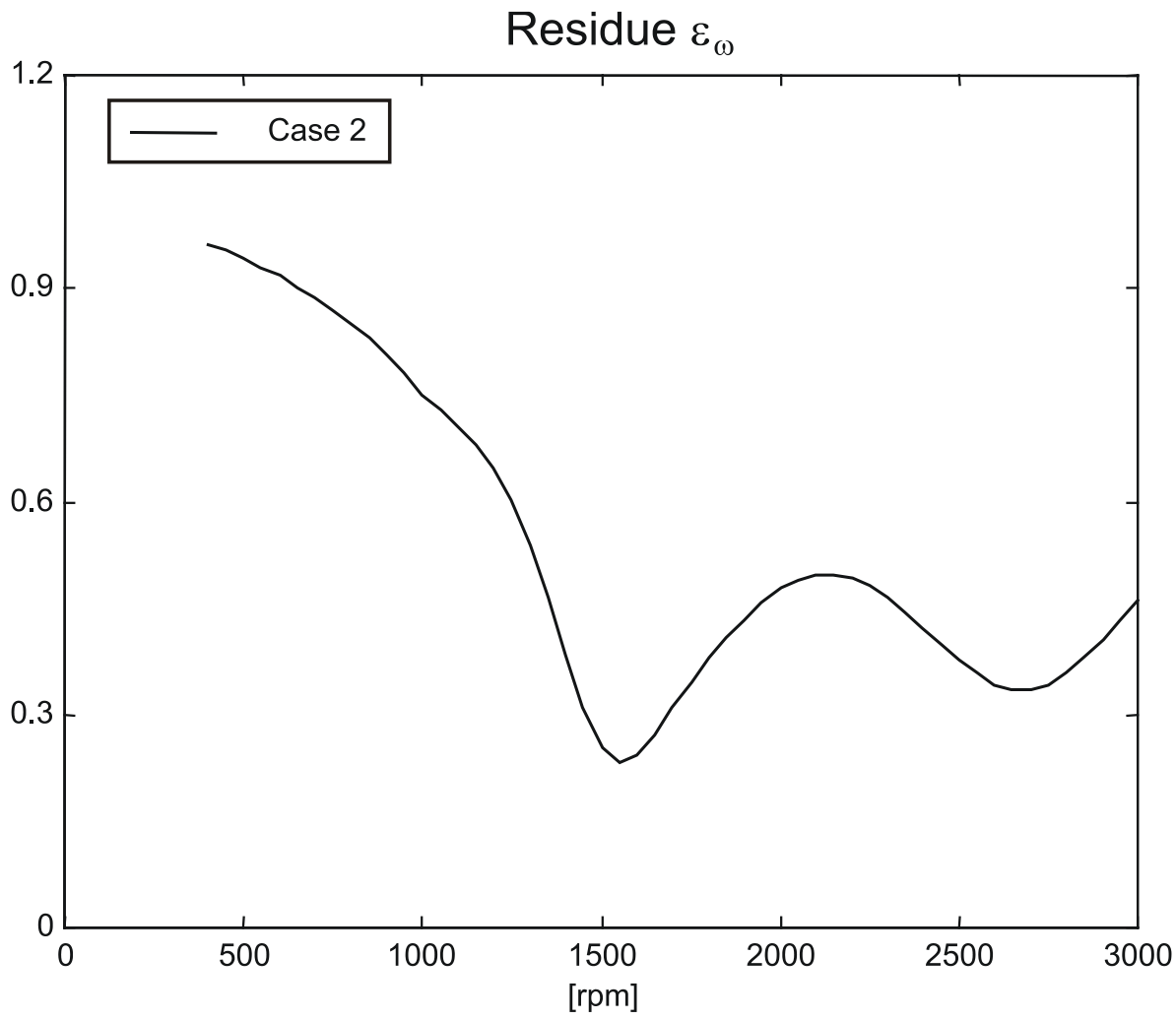

Figure 8 Dependence of residuals on rotating speed: unbalance identifications.

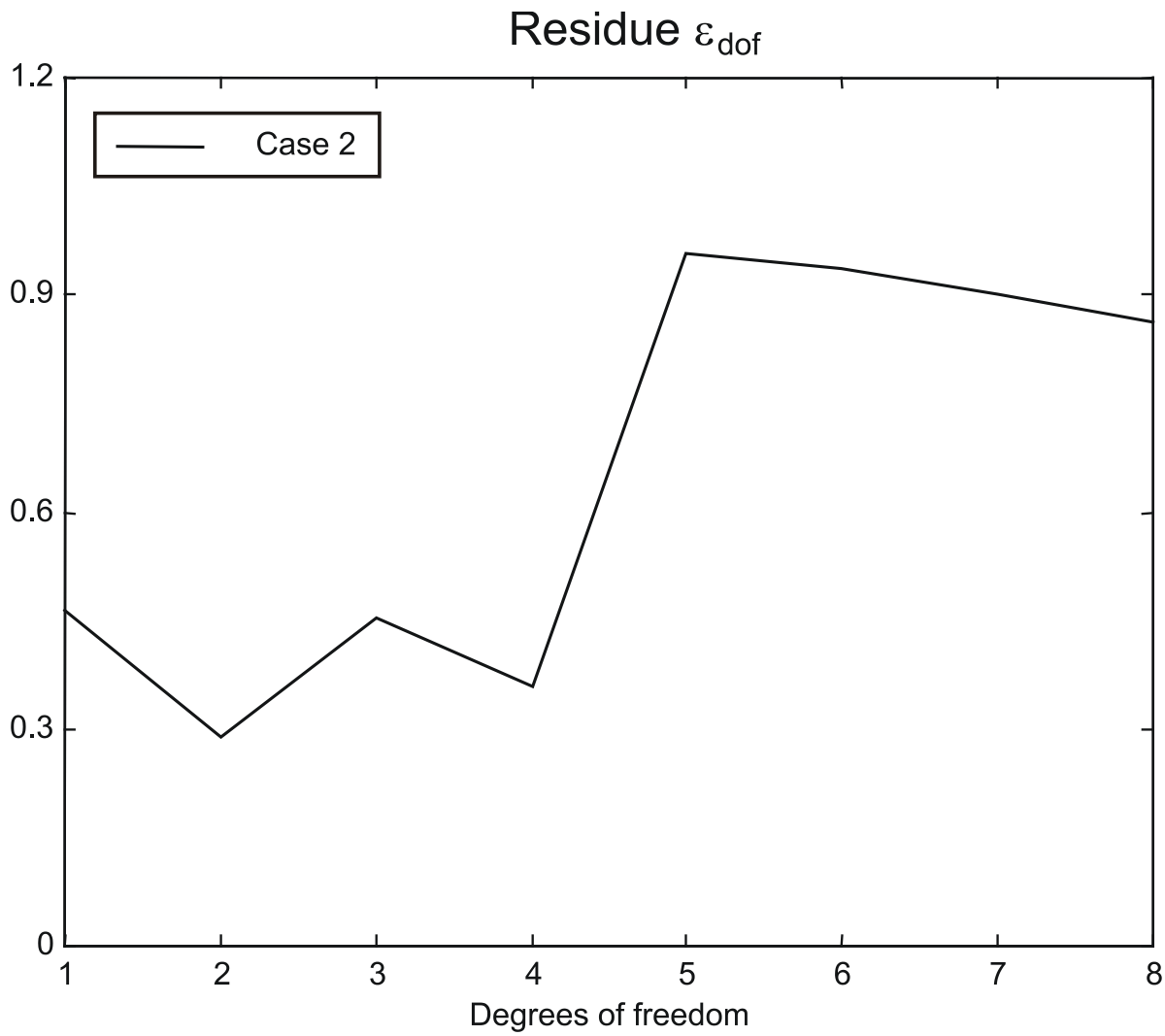

Figure 9 Dependence of residuals on d.o.f.s.

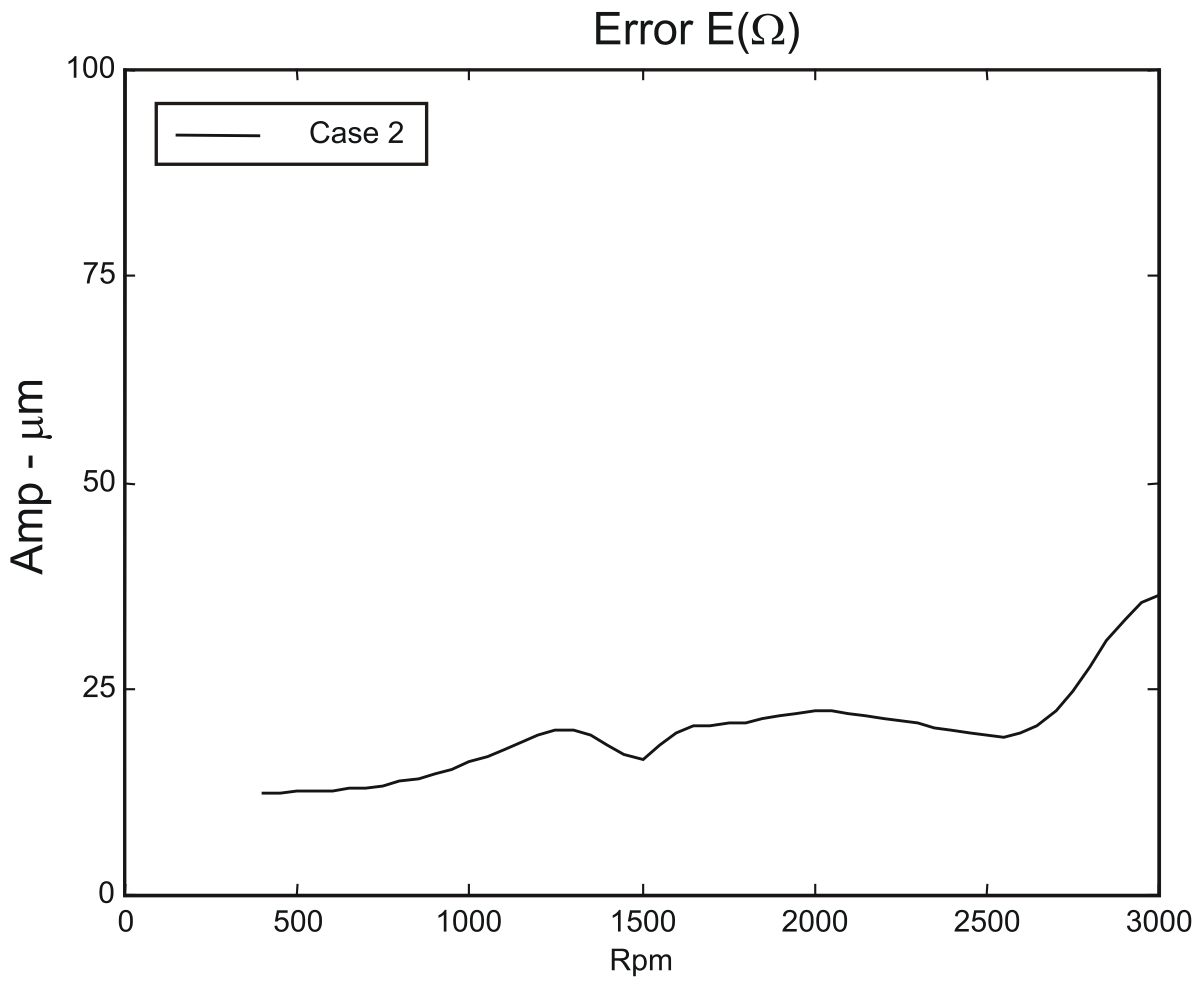

Figure 10 Absolute error $E(\Omega)$ vs. rotating speed.

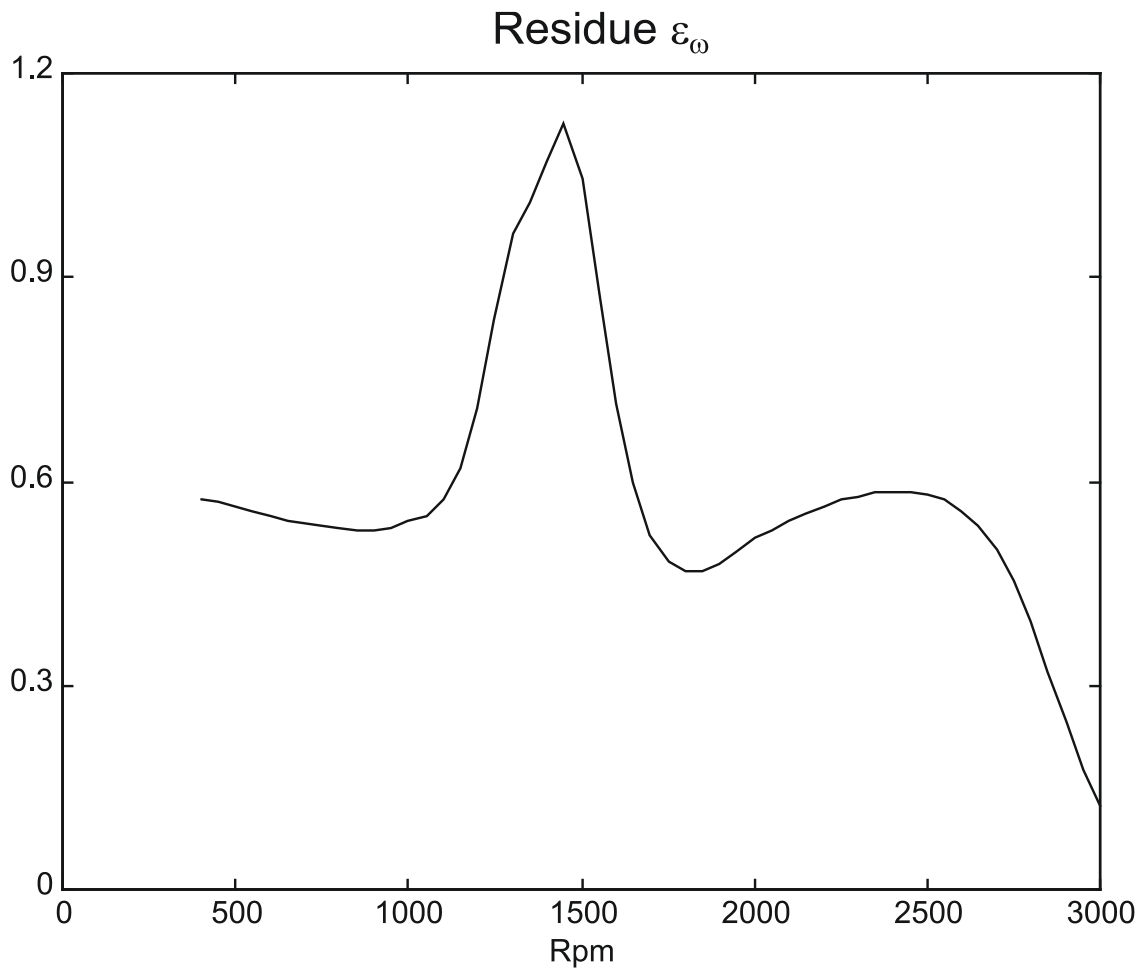

Figure 11 Dependence of residuals on rotating speed (Case 5).

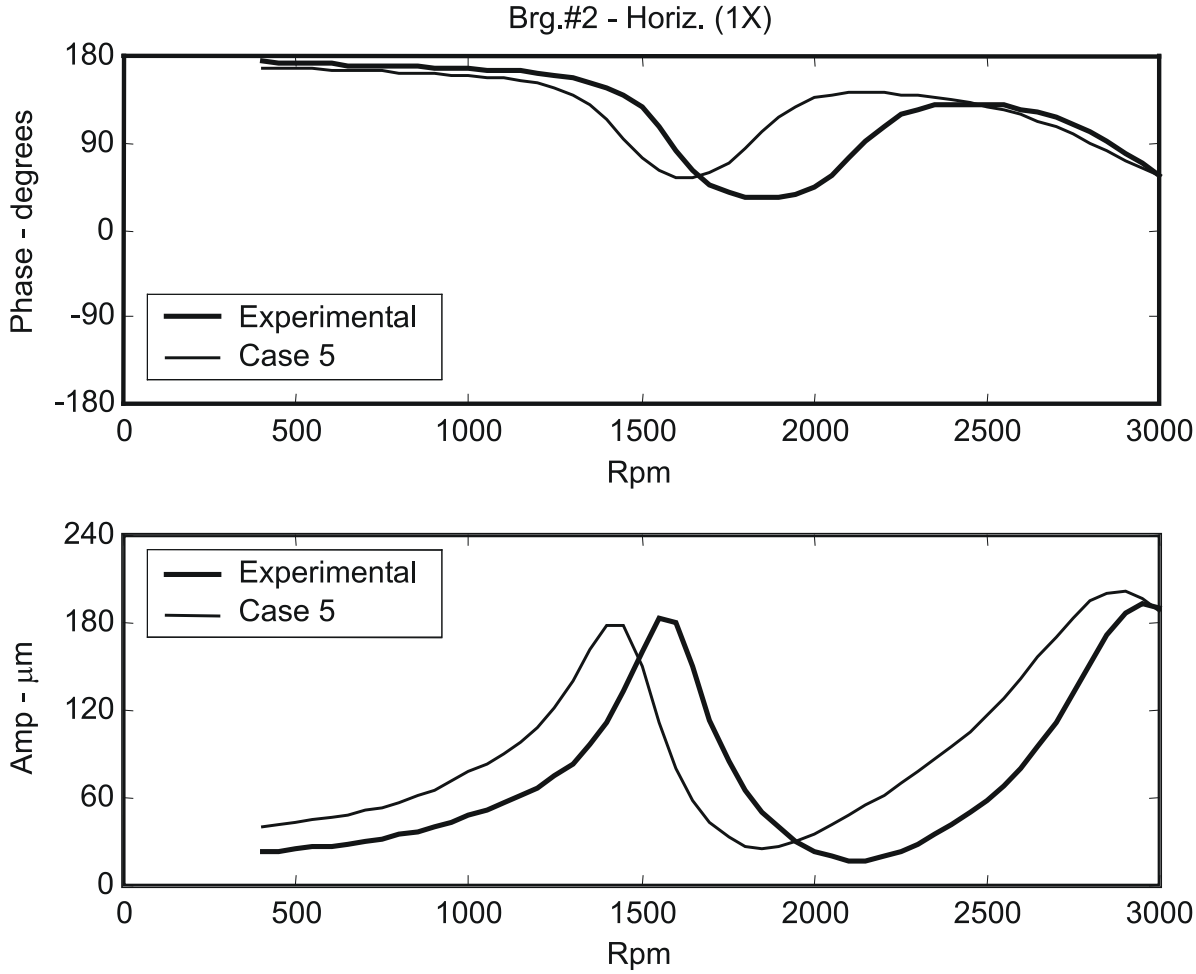

Figure 12 Bode plot of experimental and theoretical (Case 5) vibrations at brg. #2, horizontal direction.

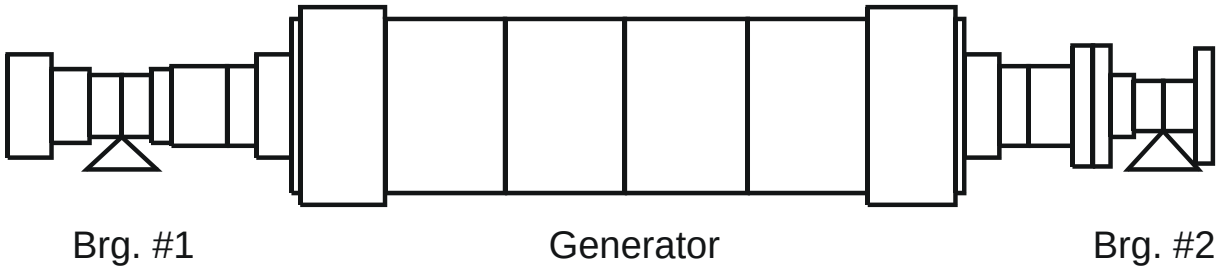

Figure 13 Finite Element model of the generator rotor.

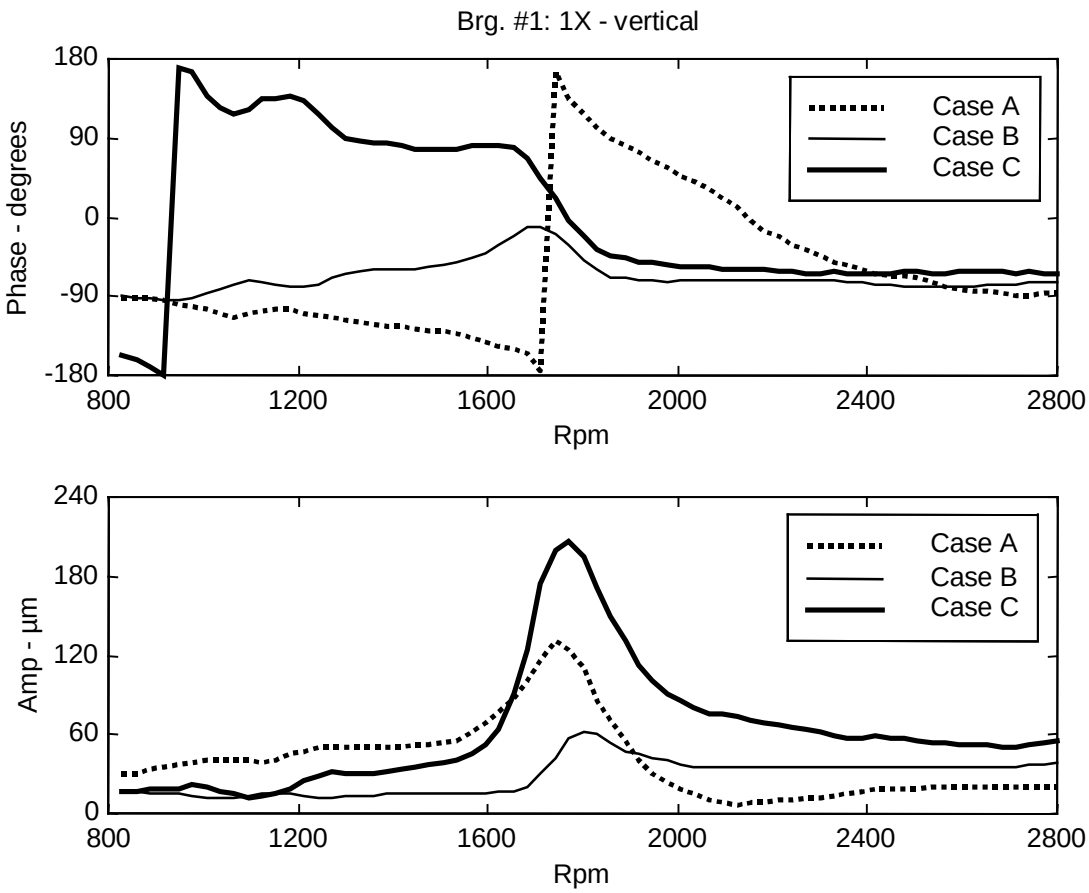

Figure 14 Bode plot of 1X transient vibrations measured on bearing #1, in vertical direction, during different speed transients (Case A: rundown, Cases B and C: runups).

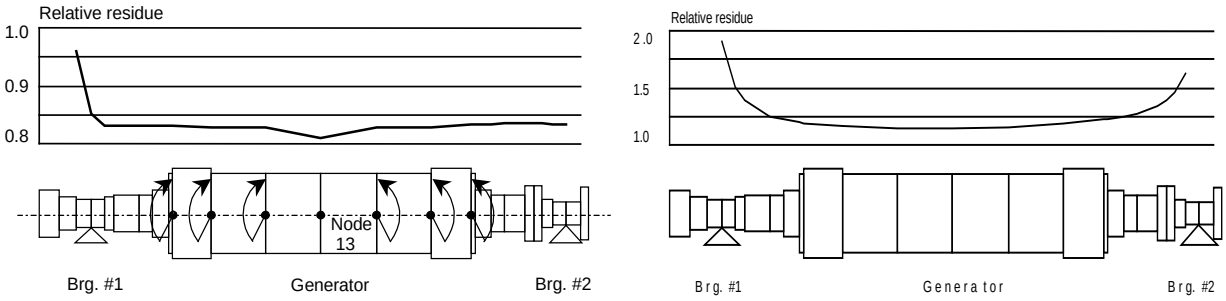

Figure 15 Dependence of the relative residual on the axial position of the two bending moments and on the position of the local unbalance.

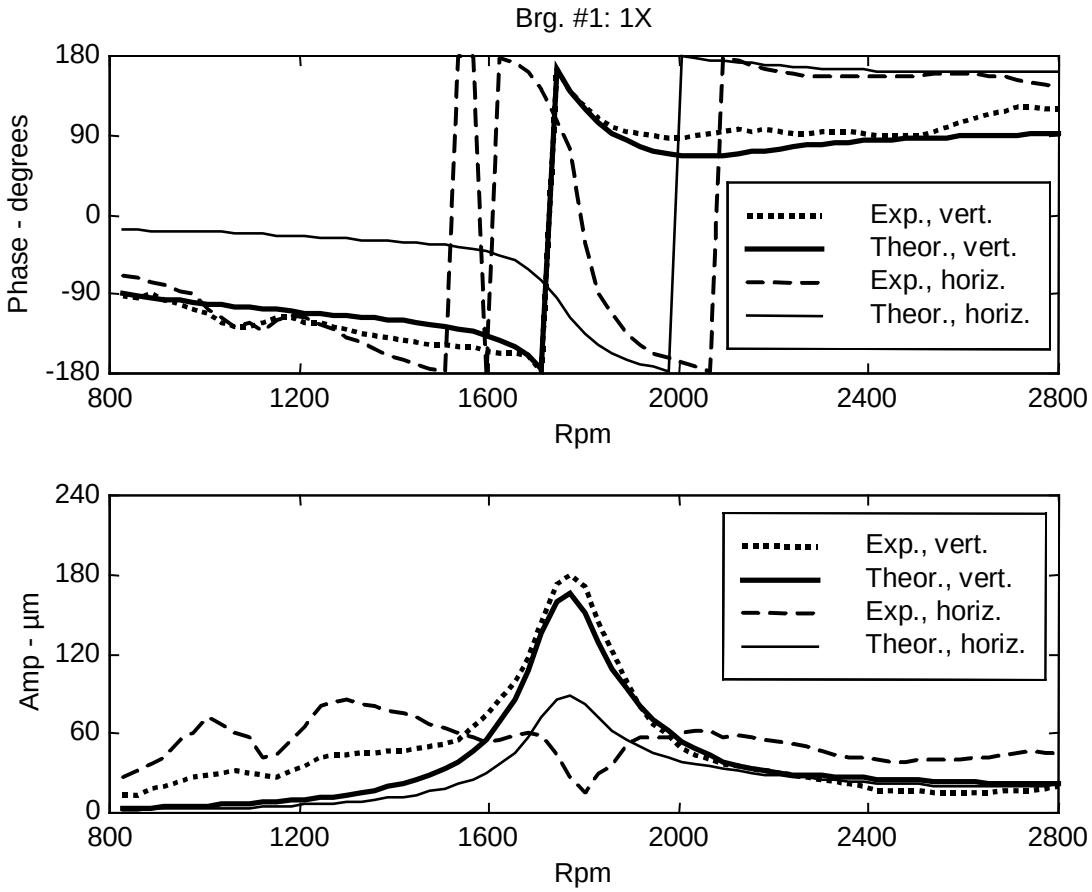

Figure 16 Comparison between the experimental 1X vibrations measured on bearing #1 and the respective numerical response obtained with the identified bending moments.

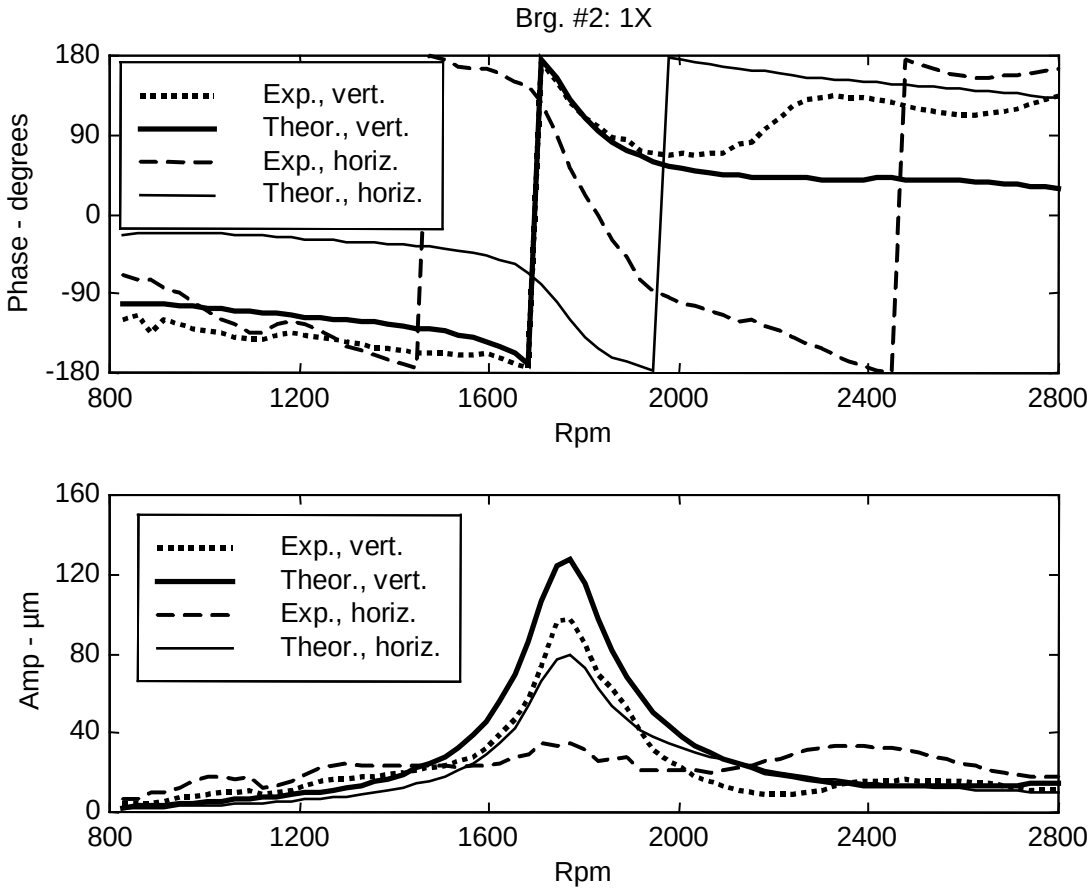

Figure 17 Comparison between the experimental 1X vibrations measured on bearing #2 and the respective numerical response obtained with the identified bending moments.

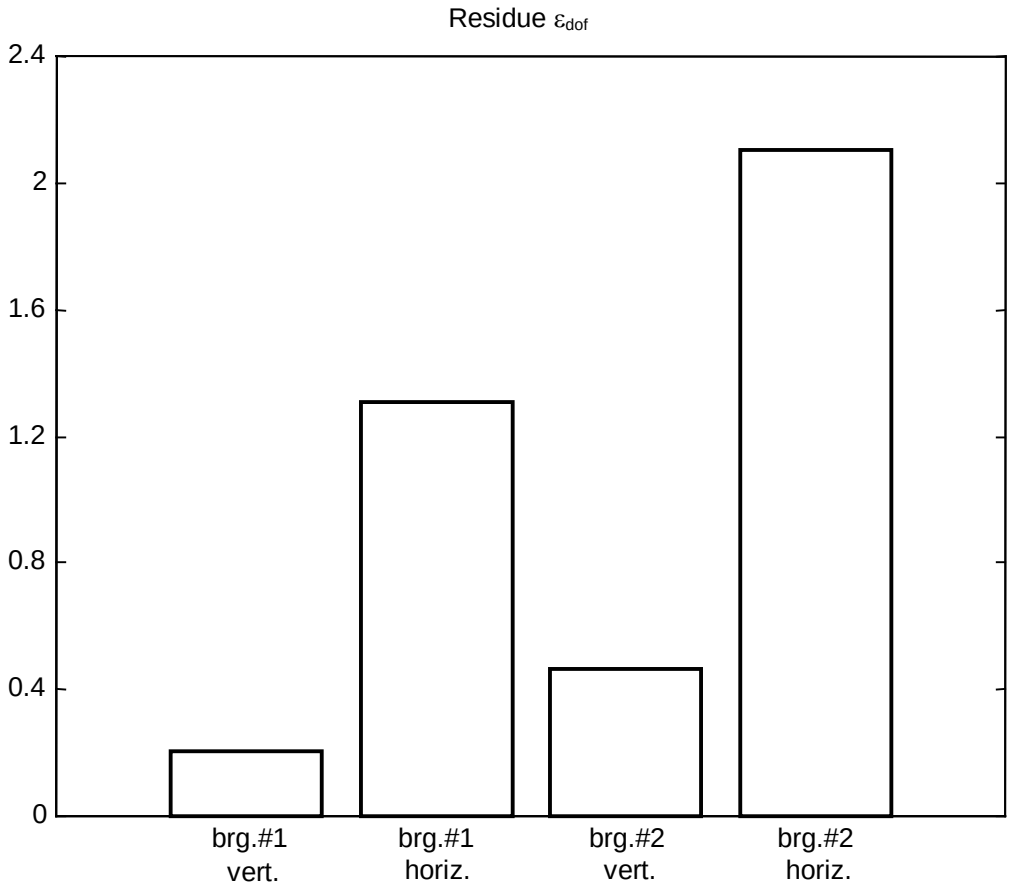

Figure 18 Dependence of the residuals, ε_{dof}, on the degree of freedom.

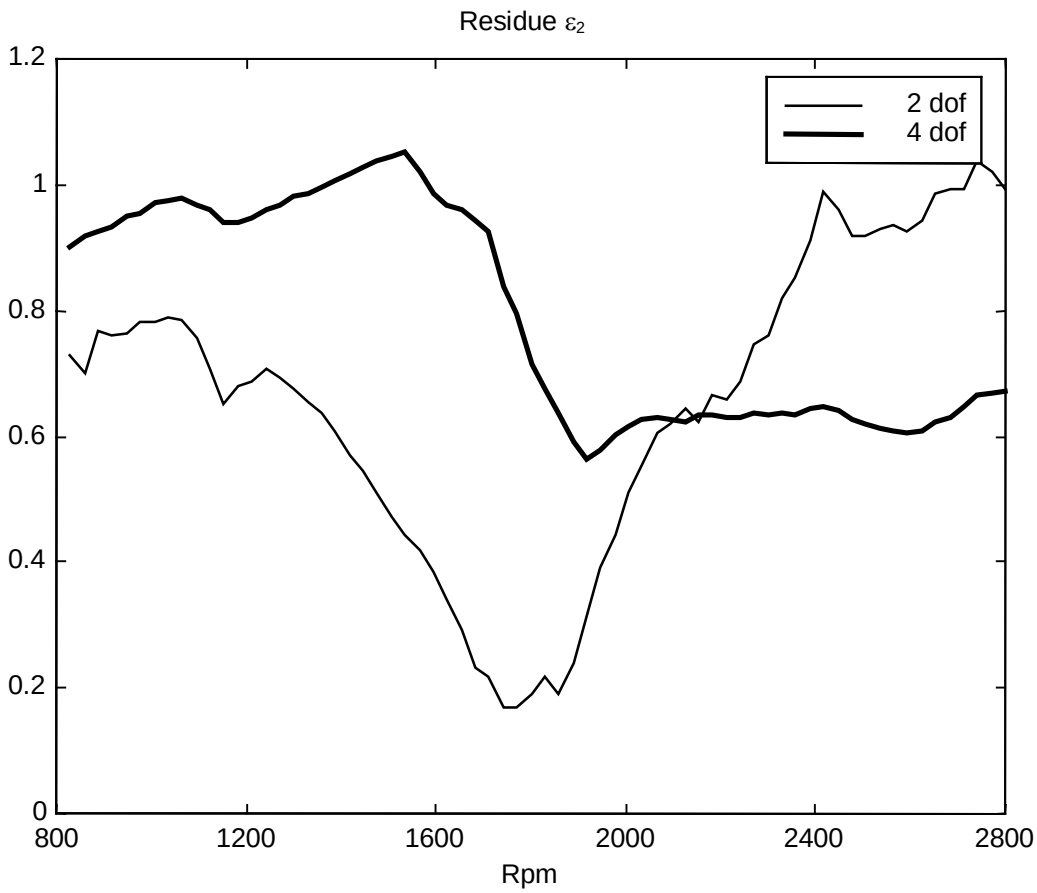

Figure 19 Dependence of the residuals ε_ω on rotating speed.

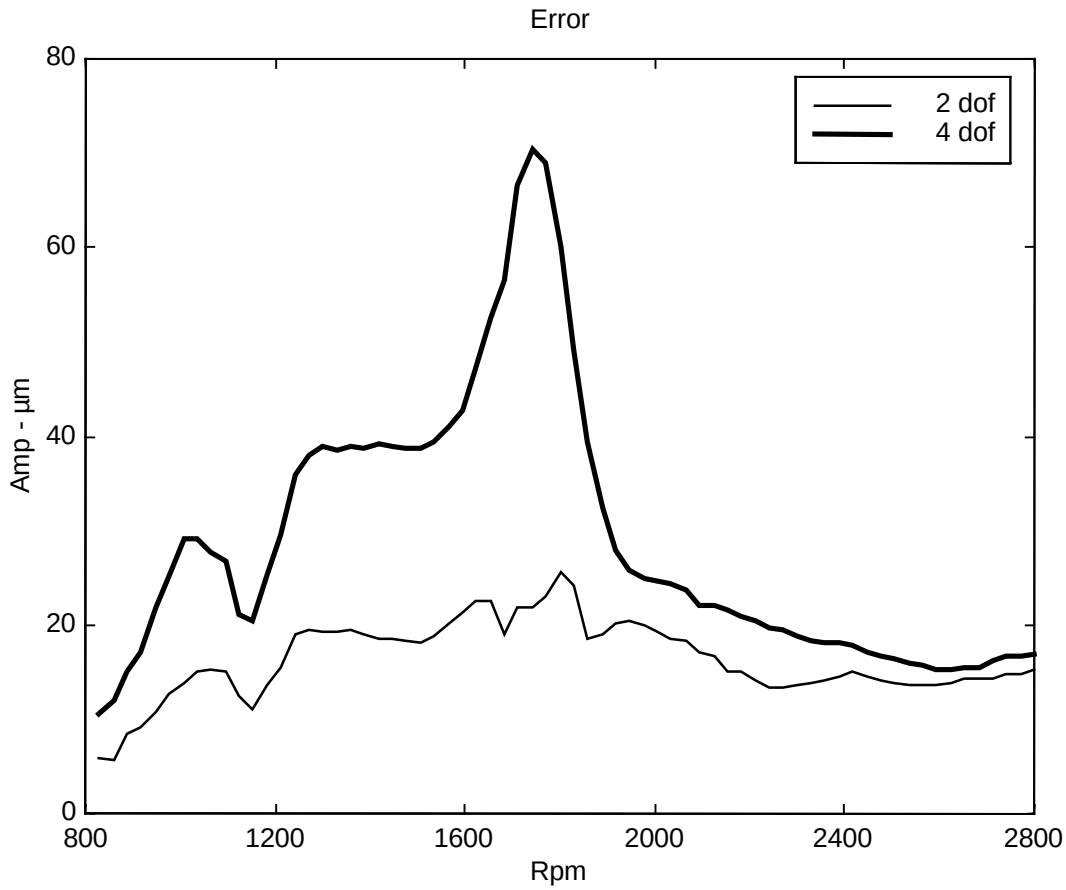

Figure 20 Absolute error vs. rotating speed.

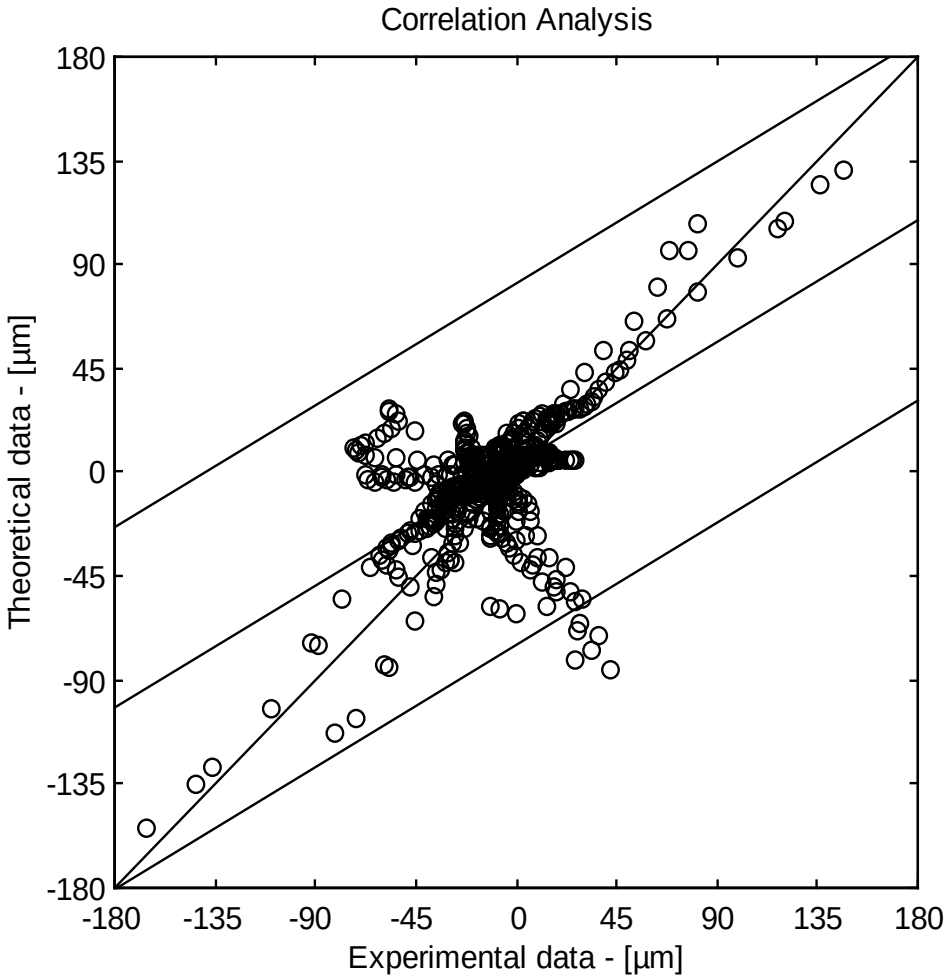

Figure 21 Regression analysis.

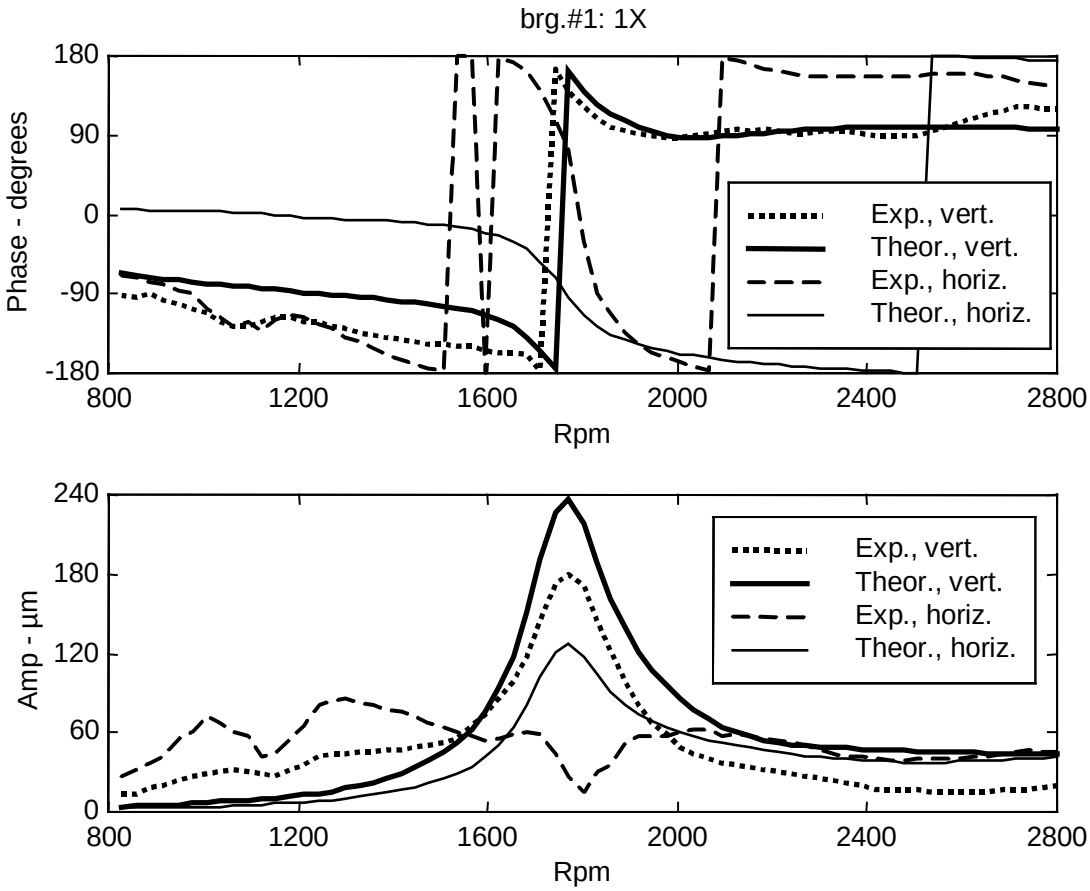

Figure 22 Comparison between the experimental 1X vibrations measured on bearing #1 and the respective numerical response obtained with the identified unbalance.

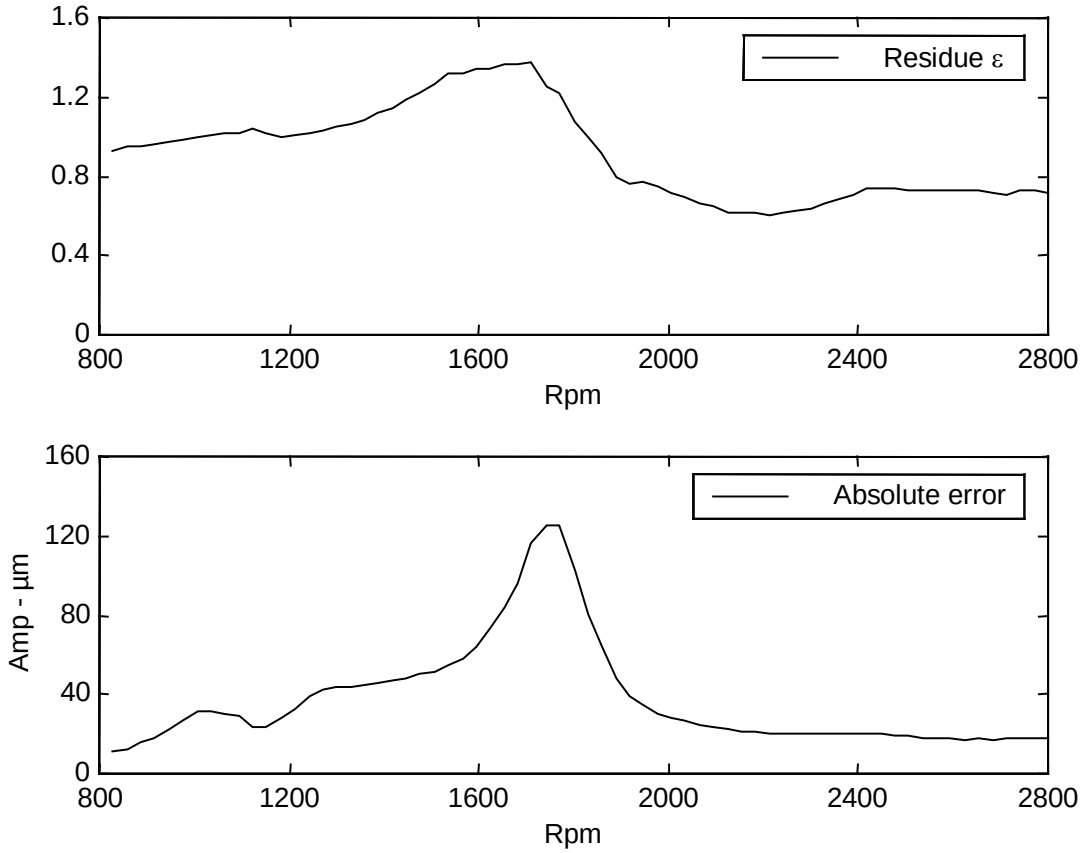

Figure 23 Relative and the absolute errors vs. the generator rotating speed.